

# Cancer Research



## Blood Flow, Oxygen and Nutrient Supply, and Metabolic Microenvironment of Human Tumors: A Review

Peter Vaupel, Friedrich Kallinowski and Paul Okunieff

*Cancer Res* 1989;49:6449-6465.

**Updated Version** Access the most recent version of this article at:  
<http://cancerres.aacrjournals.org/content/49/23/6449>

**Citing Articles** This article has been cited by 100 HighWire-hosted articles. Access the articles at:  
<http://cancerres.aacrjournals.org/content/49/23/6449#related-urls>

**E-mail alerts** [Sign up to receive free email-alerts](#) related to this article or journal.

**Reprints and Subscriptions** To order reprints of this article or to subscribe to the journal, contact the AACR Publications Department at [pubs@aacr.org](mailto:pubs@aacr.org).

**Permissions** To request permission to re-use all or part of this article, contact the AACR Publications Department at [permissions@aacr.org](mailto:permissions@aacr.org).

## Review

# Blood Flow, Oxygen and Nutrient Supply, and Metabolic Microenvironment of Human Tumors: A Review<sup>1</sup>

Peter Vaupel,<sup>2</sup> Friedrich Kallinowski, and Paul Okunieff

Department of Radiation Medicine, Massachusetts General Hospital Cancer Center, Harvard Medical School, Boston, Massachusetts 02114

## Abstract

The objective of this review article is to summarize current knowledge of blood flow and perfusion-related parameters, which usually go hand in hand and in turn define the cellular metabolic microenvironment of human malignancies. A compilation of available data from the literature on blood flow, oxygen and nutrient supply, and tissue oxygen and pH distribution in human tumors is presented. Whenever possible, data obtained for human tumors are compared with the respective parameters in normal tissues, isotransplanted or spontaneous rodent tumors, and xenografted human tumors. Although data on human tumors *in situ* are scarce and there may be significant errors associated with the techniques used for measurements, experimental evidence is provided for the existence of a compromised and anisotropic blood supply to many tumors. As a result, O<sub>2</sub>-depleted areas develop in human malignancies which coincide with nutrient and energy deprivation and with a hostile metabolic microenvironment (e.g., existence of severe tissue acidosis). Significant variations in these relevant parameters must be expected between different locations within the same tumor, at the same location at different times, and between individual tumors of the same grading and staging. Furthermore, this synopsis will attempt to identify relevant pathophysiological parameters and other related areas future research of which might be most beneficial for designing individually tailored treatment protocols with the goal of predicting the acute and/or long-term response of tumors to therapy.

## Introduction

A great number of malignancies are relatively resistant to radiotherapy, chemotherapy, and other nonsurgical treatment modalities. A variety of factors are involved in the lack of responsiveness of these neoplasms including an intrinsic, genetically determined resistance and physiological, extrinsic (epigenetic, environmental) factors primarily created by inadequate and heterogeneous vascular networks (1-5). Thus properties such as tumor blood flow, tissue oxygen and nutrient supply, pH distribution, and bioenergetic status, factors which usually go hand in hand, can markedly influence the therapeutic response. Data on these parameters are mostly derived from rodent tumors (for references see 6-12). However, fast-growing rodent tumors might not adequately represent the multitude of neoplastic growths encountered in patients. Unfortunately, data on human tumors *in situ* are scarce and there may be significant errors associated with the techniques used for measurements. This should be kept in mind when comparing available results from the literature.

In order to create a factual basis for further research, the currently available information on tumor blood flow, tissue

oxygen distribution, nutrient supply, and metabolic microenvironment is compiled in this review. This synopsis attempts to identify areas in which future research might be most beneficial (e.g., for designing specifically tailored treatment protocols for individual subjects, for assessing early tumor response to treatment, and/or for examining potentially useful tools for prediction of long-term tumor response).

## Vasculature and Blood Flow of Human Tumors

### Vascularization of Tumors

The establishment and progressive expansion of malignant tumors following the avascular growth period are possible only if convective nutrient supply and waste removal are initiated through nutritive blood flow, i.e., flow through tumor microvessels that guarantees adequate exchange processes between the microcirculatory bed and the cancer cells. When considering the origin of blood vessels in a growing tumor, one must take into account the existence of two different populations: (a) preexisting host vessels which are incorporated into the tumor tissue; and (b) tumor microvessels arising from neovascularization due to the influence of tumor angiogenesis factor(s).

In the preexisting, normal host vasculature which provides the structures from which neovascularization arises and which can fulfill microcirculatory functions for certain time periods in given locations within a tumor, a series of morphological and functional changes occur. First, the venules become tortuous, elongated, and often dilated. The host vessels per unit tumor mass do not increase in number, thus leading to a reduction of the available exchange area for oxygen, nutrients, hormones, growth factors, and waste products (e.g., hydrogen ions, lactic acid, necrosis products). During growth, some of the preexisting host vessels incorporated in the tumor mass disintegrate, are obstructed, or are compressed. The remaining vessels seem to remain functionally intact and probably maintain the ability to respond to physiological and pharmacological stimuli. This holds especially true for the arterial vessels which seem to be permanently dilated and somehow "resistant" to the invasive and destructive growth of cancer cells. Spontaneous vasomotion, a typical feature of normal tissues, is mostly lacking in tumor arterioles (for reviews see Refs. 2, 9, and 13-16).

Neovascularization in tumors usually originates from venules within the tumor mass or from venules of the host tissue adjacent to the invasion front. Vascular buds and sprouts grow out from the venular sites. These soon begin to show lumen and randomly fuse, giving rise to loops and anastomosing with arteriolar vessels. At this point blood perfusion through the newly formed microvessels can begin. Occasionally, venular sprouts anastomose with other venules, so that the newly formed vascular network is both supplied and drained by venules.

Whether or not the patterns of the newly formed vascular networks are characteristic for different tumor types is still an open question (for reviews see Refs. 17 and 18). Newly formed

Received 4/25/89; revised 7/17/89; accepted 8/14/89.

The costs of publication of this article were defrayed in part by the payment of page charges. This article must therefore be hereby marked *advertisement* in accordance with 18 U.S.C. Section 1734 solely to indicate this fact.

<sup>1</sup> Dedicated to Dr. Pietro M. Gullino, an outstanding pioneer in tumor pathophysiology, on the occasion of his 70th birthday.

<sup>2</sup> A. Werk Cook Professor of Radiation Biology/Physiology at Harvard Medical School. To whom requests for reprints should be addressed, at Department of Physiology and Pathophysiology, Pathophysiology Division, University of Mainz, D-6500 Mainz, Federal Republic of Germany.

Table 1 Relevant structural and functional abnormalities of tumor neovasculature and microcirculation

A. Structural abnormalities ("vascular chaos")	B. Functional abnormalities ("circulatory chaos")
<p>1. Abnormal vessel wall</p> <ul style="list-style-type: none"> <li>Incomplete or missing endothelial lining</li> <li>Interrupted or absent basement membrane</li> <li>Blood channels lined by tumor cell cords</li> <li>Lack of pericytes, contractile wall components, and pharmacological/physiological receptors</li> </ul> <p>2. Abnormal vascular architecture</p> <ul style="list-style-type: none"> <li>Contour irregularities (formation of lacuna-like, sinusoidal, and cystiform blood vessels)</li> <li>Tortuosity (distortions, twisting, bending)</li> <li>Elongation of vessels</li> <li>Existence of arteriovenous shunts (global flow &gt; nutritive flow)</li> <li>Loss of hierarchy</li> </ul> <p>3. Abnormal vascular density</p> <ul style="list-style-type: none"> <li>Heterogeneous distribution of vascularization ("chaotic network," appearance of avascular areas)</li> <li>Expansion of the intercapillary space (increase of diffusion distances)</li> </ul>	<p>1. Consequences of altered morphology</p> <ul style="list-style-type: none"> <li>Arteriovenous shunt perfusion (<math>\approx 30\%</math>)</li> <li>Regurgitation and intermittent flow</li> <li>Unstable speed and direction of flow</li> <li>Absence of vasomotion</li> <li>Increased vascular fragility</li> <li>Obstruction of microvessels by WBC and tumor cells</li> <li>High tumor vascular (geometric) resistance</li> </ul> <p>2. Consequences of altered rheology</p> <ul style="list-style-type: none"> <li>RBC sludging, leukocyte sticking</li> <li>Platelet aggregation</li> <li>Micro- and macrothrombosis</li> <li>Increase of viscous resistance</li> </ul> <p>3. Consequences of increased vascular permeability</p> <ul style="list-style-type: none"> <li>Hemoconcentration</li> <li>Significant interstitial bulk flow</li> <li>High interstitial fluid pressure (with compression of tumor microvessels)</li> <li>Blood cell extravasation, hemorrhage</li> <li>Increase of viscous resistance</li> </ul>

microvessels of some of the highly differentiated tumors can have a mature architecture. In contrast, the hastily formed new tumor microvessels in rapidly growing tumors show a series of severe structural abnormalities. The most relevant of these vascular abnormalities are listed in Table 1. From the fact that hypoxic and ischemic areas can be evident during very early growth stages of (xenografted) human tumors, it might be concluded that the morphological appearance of the tumor vascular bed does not necessarily allow direct judgments concerning functional aspects of the tumor microcirculation or of the nutritive blood flow. This is due to the fact that, in very early growth stages, serious functional disturbances of the microflow are already manifest. Some of these are listed in Table 1. This should be stressed, since vascular morphometry and diagnostic X-ray angiography are often improperly used for prospective estimations of tumor radiosensitivity or local pharmacokinetics. A high vascular density is a prerequisite for but is not necessarily indicative of a high nutritive flow.

There are some indications that considerable spatial and temporal heterogeneity of the microcirculation exists among individual vessels and different microareas within one tumor, in the same tumor line at different sizes or at different growth sites, between different tumor lines with the same grading and staging, as well as between tumors of different histologies.

### Tumor Blood Flow

**Perfusion Rate of Human Tumors.** Whereas blood flow rates of most isografted rodent tumors decrease with increasing tumor size, a similar relationship has not been found to be valid for all human tumors (for reviews see Refs. 6, 9, and 11). Whether the latter indicates a lack of sufficient data or a fundamental deviation from isografted tumors is unclear at this time. Considering the pathogenetic mechanisms directly responsible for the weight-adjusted flow decline that occurs with tumor growth, (a) a progressive rarefaction of the vascular bed, *i.e.*, a decrease in the number of patent vessels per g of tumor, (b) severe structural and functional abnormalities of the tumor microcirculation, and (c) the development of necrosis must be taken into account. These disturbances of tumor microcirculation are apparent even at early growth stages and, at least in iso- or xenografted rodent tumor models, become more pronounced with tumor growth (for references see Refs. 9 and 19–21). As a rule, the blood supply to animal tumors is spatially heterogeneous on both a micro- and a macroscopic scale. In

addition, there is a pronounced temporal heterogeneity within a tumor and a tremendous variability among individual tumors of the same line.

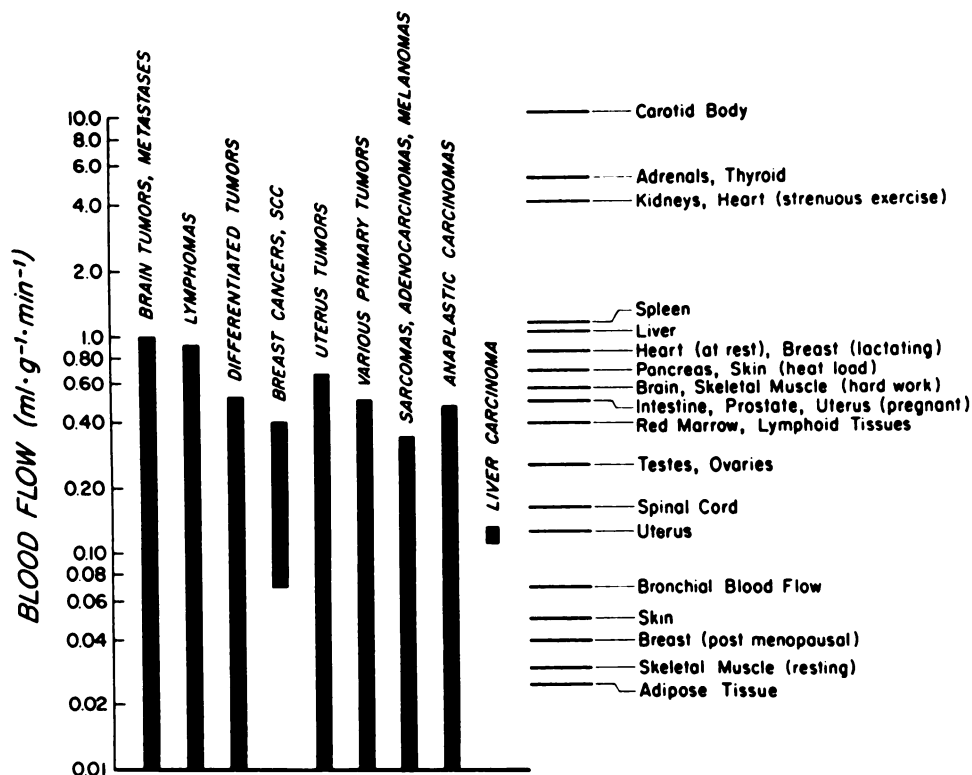
Measurements of blood flow in a series of xenotransplanted human tumors in immunodeficient animals exhibited a 10-fold variation in weight-adjusted tumor perfusion indicating large variations in angiogenesis. Flow values obtained were consistent with data from clinical observations of human tumors *in situ* and were within the range of that of normal tissues (tissues of origin) at different conditions of functional activity (22, 23). In an experimental model of a human medulloblastoma, two distinct tumor patterns were observed, depending on both histology and blood flow (24). In tumors with a solid mass of tumor cells and limited infiltration of the brain around the tumor, blood flow values were lower than in brain cortex or in the contralateral corpus callosum. In contrast, infiltrative tumors characterized by cells growing only perivascularly had blood flows significantly higher than in tumor-free white matter but lower than in normal cortex.

Global tumor perfusion (blood flow) has been measured in patients using various techniques. To date, none of the approaches used to measure tumor perfusion provide the information needed on the events occurring at the microscopic level. Furthermore, they cannot give detailed data on arteriovenous shunt perfusion. Methods used for blood flow measurements in human tumors include steady-state inhalation of  $C^{15}O_2$  and positron emission tomography,<sup>3</sup> hydrogen and isotope clearance techniques ( $^{85}Kr$ ,  $^{133}Xe$ ) and thermal washout procedures. Since in the latter case heat transport by conduction is not negligible, especially in superficial tumors, the blood flow rate calculated contains a systematic error which, under low-flow conditions, can vary between different experimental conditions and can be quite large in absolute values. In the case of isotope clearance techniques, the indicator generally is applied topically, *i.e.*, into the tumor mass, which can lead to tremendous perturbations of the local microcirculation due to an increase in intratumor pressure.

For comparison the blood supply to normal organs, and of tumors is given in Fig. 1 using specific perfusion rate units (ml/g/min) (25). These are average values, from which there may be departures in individual cases. Moreover, the specific perfusion may vary considerably in different parts of an organ (*e.g.*, renal cortex *versus* medulla, subendocardial *versus* subepi-

<sup>3</sup> The  $C^{15}O_2$  PET technique is based on the exchange of water in the tissue; thus shunt perfusion should virtually be excluded.

Fig. 1. Variability of blood flow in human malignancies (■) and mean flow values of normal tissues (horizontal lines). Pooled data are given for the various tumors: primary brain tumors and metastatic tumors in the brain; lymphomas; differentiated tumors; breast cancers and squamous cell carcinomas (SCC); uterus tumors; various primary tumors; sarcomas, adenocarcinomas, and melanomas; anaplastic carcinomas; liver carcinoma. (The respective references are given in the text.)



cardial regions of the myocardium, white matter versus gray matter of the brain), and under different conditions of activity (e.g., heart at rest or during strenuous exercise, skeletal muscle at rest or during hard work, skin in a cold environment and during heat load).

The blood flow of malignant tumors in humans has been studied using radioactive <sup>90</sup>Y microspheres while treating patients (26). In this study, the amount of blood flowing to tumors was estimated and compared to the blood supply of normal tissues at the site of tumor growth. This "qualitative" investigation demonstrated a normal tissue flow/tumor flow ratio in the range of 3/1 to 30/1. Primary tumors tended to have a better blood supply than metastatic lesions, and peripheral tumor areas showed a higher flow rate than more central portions. These data imply that tumor blood flow may be considerably lower than normal tissue perfusion. Such a conclusion, however, certainly requires a more precise understanding of tumor pathophysiology and a larger data base on human tumor blood flow.

A number of studies on blood flow through human tumors have been reported since this pioneering study in 1966. Most of them are more or less casuistic reports rather than systematic investigations; therefore definite conclusions cannot be drawn. Flow studies were performed on brain tumors (27-39), breast cancers (27, 40, 41), metastatic lesions (36-38, 42-46), anaplastic carcinomas, differentiated tumors and lymphomas (27, 47, 48), carcinomas of the uterus (49), adenocarcinomas<sup>4</sup> and squamous cell carcinomas (50, 51), melanomas (50), liver tumors (52), lymphangiomas (53), and osteosarcomas (42).

Considering all presently available data on human tumors *in situ*, the following (preliminary) conclusions can be drawn if flow data for the different tumor types are pooled: blood flow can vary considerably despite similar histological classification and primary site; tumors can have flow rates which are similar

to those measured in tachytrophic organs (*i.e.*, in organs with a high metabolic rate such as liver, heart, or brain); some tumors exhibit flow values which are even lower than those of bradytrophic tissues (*i.e.*, of tissues with a low metabolic rate such as skin, resting skeletal muscle, or adipose tissue); blood flow in human tumors can be higher or lower than that of the tissue of origin, depending in the functional state of the latter tissue (*e.g.*, average blood flow in breast cancers is substantially higher than that of postmenopausal breast and significantly lower than flow data obtained in the lactating, parenchymal breast); the average perfusion rate of carcinomas does not deviate substantially from that of sarcomas; and metastatic lesions exhibit a blood supply which is comparable to that of the primary tumors as long as comparable sizes are considered.

Due to methodological uncertainties, these preliminary conclusions should be confirmed in future studies. Blood flow measurement techniques of the future should be noninvasive and should allow for serial investigations. Current promising methodologies using radiation activation (a washout technique), NMR<sup>5</sup> and computerized body tomography, angiographic and cinematographic techniques (flow imaging techniques) and other washout procedures (*e.g.*, <sup>201</sup>Tl and D<sub>2</sub>O) may achieve this goal.

Because of a pronounced variability within tumors of a given histology, a clear correlation between tumor type and specific blood flow rate is not obvious although in some studies flow differences were significant when different tumor types or tumors with different grades were compared. In a report on regional blood flow in human malignancies, Mäntylä (47) has reported statistically higher flow values in lymphomas than in

<sup>5</sup> The abbreviations used are: <sup>31</sup>P NMR, <sup>31</sup>P nuclear magnetic resonance; HbO<sub>2</sub>, oxyhemoglobin saturation of RBC in tumor microvessels; PCR, phosphocreatine; NTP, nucleoside triphosphate; PME, phosphomonoesters; PDE, phosphodiesters; pH<sub>POT</sub>, pH values measured with the potentiometric (electrode) technique; pH<sub>PET</sub>, pH values derived from positron emission tomography; pH<sub>NMR</sub>, pH values obtained by <sup>31</sup>P nuclear magnetic resonance spectroscopy; PET, positron emission tomography; DMO, dimethylxazolidinedione.

<sup>4</sup> M. Molls, unpublished observations.

anaplastic or differentiated carcinomas. Interestingly, no correlation between the size of the tumors and the blood perfusion rates was seen. This result agrees with some single observations of Tanaka (54) and Bru *et al.* (55). Considering tumors of different grades, Nyström *et al.* (49) measured significantly different flow values in low- and in highly differentiated carcinomas of the corpus uteri (0.4 versus 0.1 ml/g/min). However, blood flow variability may not necessarily correlate with tumor grade since astrocytomas of different grades exhibited similar mean flow values and great intertumor variability within one grade (see Table 2). In general, perfusion through astrocytomas was found to be extremely variable, but the mean value was close to that of the contralateral white matter. Flow ranged from virtually zero to values in excess of normal gray matter. No relationship between tumor perfusion and vascularity was found in a series of patients. This suggests that vascularity as judged by histological examination or angiography is an inadequate method of assessing nutritive blood flow (27, 36). In addition, the tumor size seems to have no significant influence on the specific perfusion rate of most tumors investigated to date (47).

Blood flow through tumors is anything but uniform. Most tumors contain both highly perfused areas, which are rapidly growing and which infiltrate the normal surroundings, and regions with compromised and sluggish perfusion, often associated with the development of necrosis.

**Arteriovenous Shunt Perfusion in Tumors.** First rough estimations concerning the arteriovenous shunt flow in malignant tumors showed that at least 30% of the arterial blood can pass through experimental tumors without taking part in the microcirculatory exchange processes (59–61). In patients receiving intraarterial chemotherapy for head and neck cancer, shunt flow is reported to be 8–43% of total tumor blood flow, the latter consistently exceeding normal tissue perfusion of the scalp (51). The mean fractional shunt perfusion of tumors was  $23 \pm 13\%$  (SE) in studies utilizing  $^{99m}\text{Tc}$ -labeled macroaggregated albumin (diameter of the particles, 15–90  $\mu\text{m}$ ). The significance of this shunt flow on local pharmacokinetics, on the development of hypoxia, and on other relevant metabolic phenomena has not yet been studied systematically and remains speculative. For example, oxygen diffusion distances in poorly perfused human breast cancer xenografts using tumor-specific *in vivo* data have recently been evaluated by Groebe and Vaupel (62). In this study evidence is given that radiosensitivity may be less than 10% of maximum at intercapillary distances above 100  $\mu\text{m}$ ; if intercapillary distances exceeded 140  $\mu\text{m}$ , areas of radiobiological hypoxia extended to the arterial end of the microvessel. These calculations predict that the radiobiologically hypoxic cell fraction in those tumors would be increased by 4% (or 8%) if a shunt perfusion of 20% (or 35%) is assumed.

**Physiological and Pharmacological Responsiveness of Tumor Blood Vessels.** Another open question deals with the respon-

siveness or reactivity of tumor microvessels to physiological and pharmacological stimuli. As already indicated, it is most likely that only the incorporated host vessels still exhibit some reactivity. Therefore, the existence and the extent of a microcirculatory regulation and the overall response of a tumor will depend on the prevalence as well as on the proportion of residual normal host vessels in a growing tumor. Most probably the vessels recruited from the preexisting vascular network are maximally dilated in poorly perfused tumors (as a result of tissue acidosis and hypoxia/anoxia). The ratio of host vessels to newly formed vessels can vary from one location to another and from one observation time to the next in the same tumor and from one tumor to another (19). Intratumor responsiveness can be feigned by steal phenomena and anti-steal phenomena in conjunction with the vascular bed of the normal host tissues adjacent to the tumor tissue.

The principle parameters determining the actual blood flow rate through the tumor vascular network are (a) perfusion pressure, (b) geometric resistance (governed by the vessel diameter), and (c) the viscous resistance which is determined predominantly by the rheological properties of the blood (19–21, 63). Hence, modifications of these three parameters may have the potential to modulate tumor blood flow rate. Whether or not a treatment advantage can be gained using the differential response of tumor blood flow to chemical (or pharmacological) agents is still an open question. Encouraging research results with some agents were obtained in animal studies and require clinical testing. Measurements of the vascular responsiveness of human tumors have been anecdotal, generally estimated via angiograms during diagnostic procedures. Effects of various vasodilators, of vasoconstrictors, and of chemical substances which can alter blood viscosity have been comprehensively reviewed by Jain and Ward-Hartley (6), Vaupel (9), Peterson (64), and Jirtle (65). The evidence presented in these reviews shows tremendous disparity making definitive conclusions impossible at the present time.

**Convective Currents in the Interstitial Space of Tumors.** Bulk flow of free water in the interstitial space of tumors is another characteristic pattern of malignant growth. Due to a high vascular permeability and due to the absence of a functioning lymphatic drainage system in many malignant tumors, there is a significant bulk flow of fluid in the interstitial space. Whereas in normal tissues, convective currents in the interstitial space are estimated to be about 0.4–1% of plasma flow, in isografted rat tumors bulk flow of free fluid was 3–7% of the plasma flow rate (19, 66). In xenografted human tumors interstitial water flux can be as high as 7–14% of the respective plasma flow (67). A significant hemoconcentration during tumor passage and thus a tremendous increase in viscous resistance is an obligatory consequence. This has been shown for both isografted rodent tumors (68, 69) and xenografted human tumors (22). This pronounced bulk transfer of fluid in the interstitial space is accompanied by a high interstitial fluid pressure in the respective tumors which can cause a progressive vascular compression with growth (for a review see Ref. 66). Very likely the same holds true for tumors in patients, although this has not yet been shown experimentally.

## Oxygen Consumption Rates and Tumor Tissue Oxygenation

### *Oxygen Consumption Rates of Human Tumors in Situ*

Cellular respiration was among the first processes to be investigated in early cancer biochemistry. The studies of War-

Table 2 Blood flow through normal human brain and through primary and metastatic brain lesions (pooled data)

Tissue	Blood flow (ml/g/min)	Refs.
Astrocytomas		
Grade I	0.03–0.43	} 28, 35, 37–39
Grade II	0.03–1.01	
Grade III	0.26–0.98	
Grade IV	0.15–1.02	
Brain metastases	0.03–0.72	28, 33, 37, 38
Normal gray matter	0.25–0.78	} 27, 28, 33, 34, 37,
Normal white matter	0.08–0.33	

burg (70) resulted in his formulation of a pattern essential for malignancies, namely, an impaired respiratory rate of the tumor tissue, a partial failure of the Pasteur effect, and an excessive rate of aerobic glycolysis, *i.e.*, the formation of lactic acid from glucose in the presence of oxygen. Subsequent studies indicated, however, that these notions were neither characteristic nor unique to malignant tumors (*e.g.*, aerobic glycolysis is also found in the renal medulla, in the retina, in leukocytes, and in other phagocytic cells). Oxygen consumption rates of tumors *in vivo* are intermediate between normal tissues with low metabolic rates and normal tissues with quite high activities (Fig. 2). The same holds true for the oxygen utilization; *i.e.*, O<sub>2</sub> extraction is not impaired and respiratory function of cancer cells is not deficient (see Table 3). For comprehensive studies on the respiration rate of human tumor tissues *ex vivo* see the reports of Aisenberg (72), Alvarez *et al.* (73), Constable *et al.* (74), Macbeth and Bekesi (75), and Shapot (76).

**Tumor Tissue Oxygenation**

As already mentioned, tissue oxygenation is one of those factors which define the cellular microenvironment and which are known to be able to modulate the sensitivity of cancer cells to certain nonsurgical treatment modalities. As a rule, tissue oxygenation is the resultant of the oxygen availability (nutritive blood flow × arterial O<sub>2</sub> concentration) and the actual respiration rate of the cells. The arterial O<sub>2</sub> concentration is mostly determined by the O<sub>2</sub> partial pressure of the arterial blood, the shape of the O<sub>2</sub> dissociation curve, the hemoglobin concentration, and the temperature of the blood (25). Release of O<sub>2</sub> from the RBC into the tissues is mostly dependent on the shape of the O<sub>2</sub> dissociation curve (which can be shifted through changes of pH, CO<sub>2</sub> partial pressure, and temperature *etc.*), the fluidity of RBC and the O<sub>2</sub> partial pressure (pO<sub>2</sub>) gradient between the blood and the surrounding tissue. Diffusional flux (*m*) within

the tissue is directly proportional to the difference in O<sub>2</sub> partial pressures ( $\Delta P$ ), to Krogh's diffusion coefficient (*K*), and the exchange area (*A*) and inversely proportional to the diffusion distance (*x*).

$$m = K \cdot A \cdot \Delta P / \Delta x \quad (\text{Fick's first law of diffusion}) \quad (A)$$

Krogh's diffusion constant is defined as

$$K = D \cdot \alpha \quad (\text{ml O}_2 \cdot \text{cm}^{-1} \cdot \text{min}^{-1} \cdot \text{atm}^{-1}) \quad (B)$$

and has been measured for tumor tissue within the temperature range of 20–40°C. It has been shown to correspond to values of normal tissue with similar water content (77, 78; *D* = O<sub>2</sub> diffusion coefficient,  $\alpha$  = O<sub>2</sub> solubility coefficient).

In normal tissues the oxygen supply meets the requirements of the cells. This is accomplished by modulating tissue blood flow and/or by changing the O<sub>2</sub> utilization (or O<sub>2</sub> extraction) in accordance with alterations in physiological conditions.

$$\text{O}_2 \text{ utilization} = \frac{\text{O}_2 \text{ consumption}}{\text{O}_2 \text{ availability}} \quad (C)$$

or

$$\text{O}_2 \text{ utilization} = \frac{\text{Arteriovenous O}_2 \text{ concentration difference}}{\text{Arterial O}_2 \text{ concentration}} \quad (D)$$

In poorly perfused tumors, modulations of both mechanisms are rather limited. For this reason, O<sub>2</sub> deficiency is a common feature in those malignancies.

Besides mathematical evaluations of the pO<sub>2</sub> distribution in tissues, polarographic and cryospectrophotometric microtechniques have been used to gain an insight into the oxygenation of tissue microareas. Utilizing O<sub>2</sub>-sensitive invasive microelectrode techniques, the pO<sub>2</sub> distribution has been measured in normal tissues and tumors of patients. In contrast, the spectro-

Fig. 2. Range of oxygen consumption rates ( $\dot{V}_{O_2}$ ) of various human malignancies (■) and of the respective normal tissues (□). Consumption data are pooled values obtained with the <sup>15</sup>O<sub>2</sub> inhalation technique and positron emission tomography (25, 27, 28, 33, 37, 40, 56). A, astrocytomas; B, gliomas; C, metastatic tumors in the brain; D, breast cancers; E, normal white matter; F, normal gray matter; G, normal breast (postmenopausal).

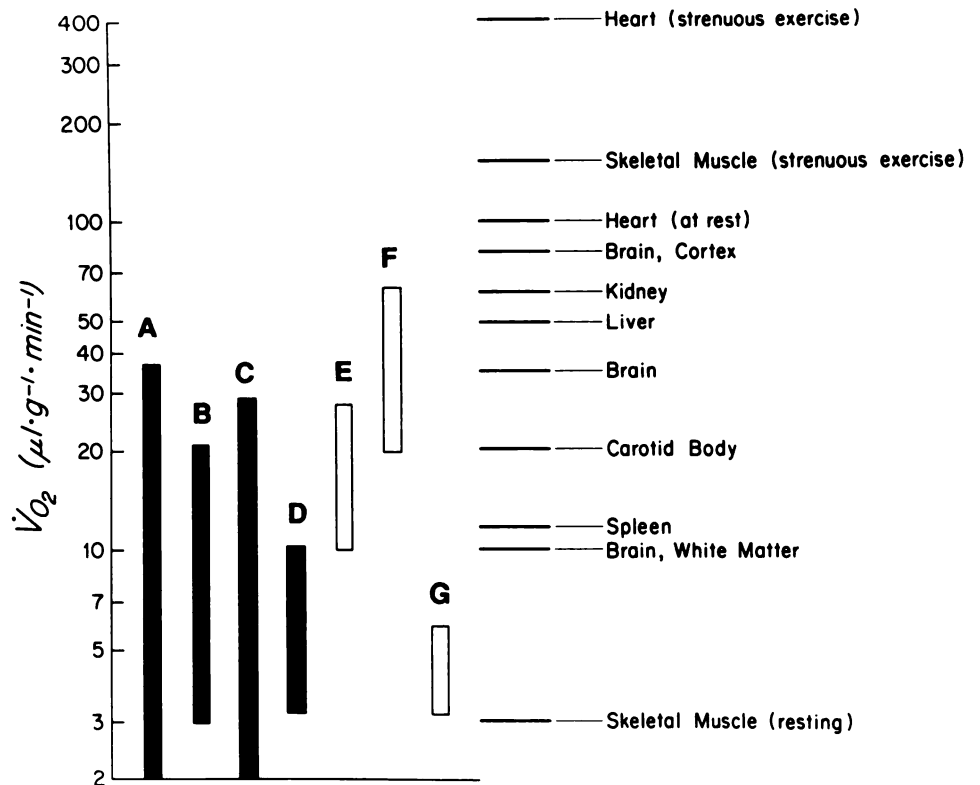


Table 3 Oxygen utilization ( $O_2$  extraction ratio,  $O_2$  extraction fraction) of human tumors and normal tissues

Tissue	$O_2$ utilization (v/v)	Refs.
Astrocytomas	0.03–0.52 <sup>a</sup>	28, 33, <sup>b</sup> 37, 39
Brain metastases	0.17–0.55 <sup>a</sup>	28, 33, <sup>b</sup> 37
Hodgkin's lymphomas (spleen)	0.10	71
Breast cancers	0.10–0.35 <sup>a</sup>	27, 40
<b>Brain</b>		
Whole	0.35–0.47 <sup>a</sup>	27
Gray matter	0.30–0.35	25
White matter	0.30–0.68 <sup>a</sup>	33 <sup>b</sup>
Gray matter	0.37–0.67 <sup>a</sup>	28, 37, 39, 56 <sup>b</sup>
White matter	0.45–0.50	
White matter	0.25–0.35	
Skeletal muscle	0.45–0.75	
Spleen	0.05	
Kidney	0.08–0.10	
<b>Heart</b>		
At rest	0.50–0.75	25
Strenuous exercise	0.85	
<b>Liver</b>		
Portal vein	0.20–0.25	
Hepatic artery	0.40–0.50	
Carotid body	0.01	
Breast (postmenopausal)	0.50–0.75 <sup>a</sup>	40

<sup>a</sup> PET study ( $^{15}O_2$ ).

<sup>b</sup> Oxygen utilizations are most probably overestimations since these studies did not correct for intravascular activity.

photometric microtechnique enables the measurement of the  $HbO_2$  of individual RBC within microvessels ( $\phi < 12 \mu m$ ) of cryobiopsies taken from patient malignancies and from the normal tissue of origin.

**Oxygen Partial Pressure Distribution.** Oxygen partial pressure distributions for isotransplanted tumors have been described in detail (11, 79, 80). In general, as a result of a compromised and anisotropic microcirculation, most of these malignancies reveal hypoxic and anoxic tissue areas which are heterogeneously distributed within the tumor mass. In poorly perfused human tumor xenografts, hypoxic ( $pO_2 < \text{normal}$ ) and anoxic ( $pO_2 = 0 \text{ mm Hg}$ ) regions were already present at early growth stages and expanded with tumor growth (22, 23). In contrast, s.c. human tumor xenografts with high perfusion rates have tissue oxygenations comparable to those of most normal organs. This is most probably due to an adequate vascularization of the latter tumors (23). Only at larger sizes did these tumors "outgrow" their vasculature and hypoxic/anoxic tissue areas develop.

When size-dependent changes in the  $O_2$  partial pressure distribution and in the tumor energy status of a murine fibrosarcoma (FSaII) and a mammary adenocarcinoma (MCAIV) were investigated *in vivo* using conscious animals and biologically relevant tumor sizes, a progressive loss of PCr and NTP with increasing  $P_{i,i}$ , PME, and PDE signals together with a decline of the median (or mean) tissue  $pO_2$  values was observed during growth (81, 82). When the mean  $pO_2$  values were plotted against the NTP/ $P_{i,i}$ , PCr/ $P_{i,i}$ , PME/ $P_{i,i}$ , and PDE/ $P_{i,i}$  ratios for tumor groups of similar mean volumes, a highly significant positive correlation was observed. From these results, it was concluded that  $^{31}P$  NMR spectroscopy can be used to indirectly evaluate tumor tissue oxygenation. Furthermore, the close correlation between tumor tissue oxygen distribution and bioenergetics suggests that the microcirculation of these murine tumors yields an  $O_2$ -limited energy metabolism.

Frequency distributions of measured  $pO_2$  values ( $pO_2$  histograms) for various normal human tissues are given in Fig. 3.

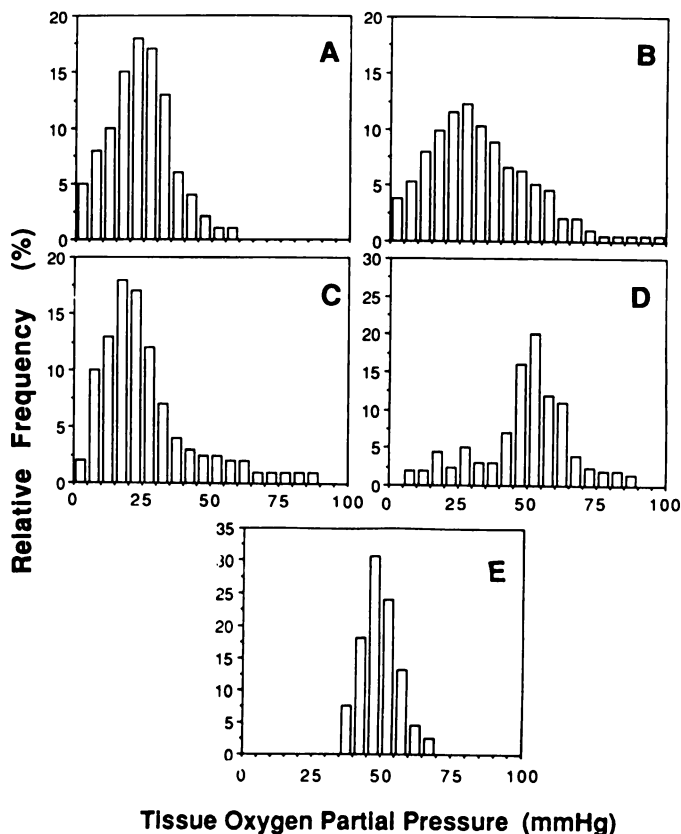


Fig. 3. Frequency distributions of measured oxygen partial pressures ( $pO_2$  histograms) for various normal tissues. A, liver; B, skeletal muscle; C, brain; D, subcutis; E, gastric mucosa (pooled data; for references see Table 4).

Table 4 Median  $pO_2$  values in various normal tissues and in tumors of patients

Tissue	Median $pO_2$ (mm Hg)	Refs.
Spleen	66 <sup>a</sup>	83
Subcutis	50	84–89
Gastric mucosa	47	90
Uterine cervix	36	91
Skeletal muscle	28	92–95
Myocardium	25	96
Liver	24	97
Brain	24	98–100
<b>Cervix cancers</b>		
Stage 0	20	91
Stage I	13	91
Stage II	5	91, 101
Adenocarcinomas	10–12	86, 90
Squamous cell carcinomas	15	84, 86, 87, 102
Breast cancers	17	84, 88, 102–104

<sup>a</sup> Arterial  $pO_2 = 100 \text{ mm Hg}$ .

As expected, there is a scattering of the tissue  $pO_2$  values between 1 mm Hg and values typical for arterial blood (80–100 mm Hg). The median  $pO_2$  values for some normal tissues are given in Table 4. Whereas in these normal tissues the medians range from 24 to 66 mm Hg, in malignancies the respective values in all malignancies analyzed thus far are  $\leq 20 \text{ mm Hg}$ . On comparison of the  $pO_2$  histograms of normal tissues with those of squamous cell carcinomas, breast cancers, or stomach cancers (see Fig. 4) there is clear evidence that in tumors there is a distinct shift of the distribution curve to the left; on the average, the mean  $pO_2$  values are lower in malignancies than in surrounding normal tissues (see Table 5), there is less scattering of the  $pO_2$  values due to lacking high  $pO_2$  values, and there is an accumulation of  $pO_2$  values in the lower  $pO_2$  classes indicating tissue hypoxia and thus reduced radiosensitivity in tumors.

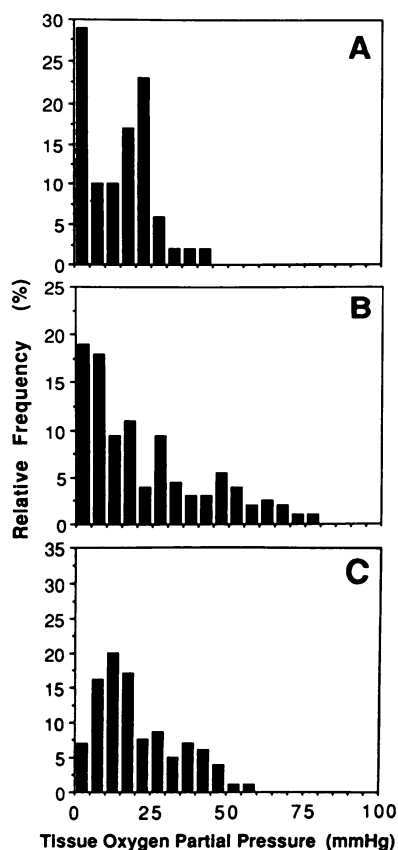


Fig. 4. pO<sub>2</sub> histograms for squamous cell carcinomas (A), breast cancers (B), and a gastric adenocarcinoma (C). Pooled data are given for the different tumor types (for references see Table 4).

Table 5 Comparison between the mean pO<sub>2</sub> values in normal tissues and in human malignancies

Tumor type	pO <sub>2</sub> (normal tissue)/ pO <sub>2</sub> (tumor) <sup>a</sup>	Refs.
Cervix cancer		
Stage 0	1.6	91
Stage 1	2.4	91
Stage 2	3.2	91
Stage 2	1.4–1.8	101
Squamous cell cancers	1.7	105
	2.4	106
	2.5	84
	4.4	86
	6.3	107
Breast cancer	1.4	88
	2.0	105
	2.4	84
	4.4	107
Melanomas	6.3–6.7	86, 106, 107
Soft tissue sarcomas	2.8	107
	6.3	86
Malignant lymphomas	1.5	105
	2.2	106
Adenocarcinomas	7.1	86
Basal cell epitheliomas	5.6	107

<sup>a</sup> Ratio of mean O<sub>2</sub> tension in normal tissue to mean O<sub>2</sub> tension in tumors.

On the basis of distributions such as those presented in Fig. 4 one can estimate the fraction of tumor cells that have reduced radiation sensitivity induced by their poor oxygenation status (*i.e.*, the radiobiologically hypoxic cell fraction). Specifically, cells in environments with pO<sub>2</sub> values below those found in venous blood will have less than maximum radiation sensitivity,

and less than 3–4 mm Hg will have a 2-fold or greater reduction in sensitivity compared to well oxygenated tissues (see Fig. 5).

The changes in the tissue pO<sub>2</sub> distribution of cervix cancers at different growth stages are shown in Fig. 6. Whereas in the normal cervical mucosa the median pO<sub>2</sub> is 36 mm Hg (7), in cervical cancers it drops to 20 mm Hg at stage 0, to 13 mm Hg at stage I, and to 5 mm Hg at stage II (91, 101). Concurrent with this lowering of the median pO<sub>2</sub> values, the pO<sub>2</sub> histogram is tilted to the left and limited in variability compared to the normal cervix mucosa. These data are indicative of an inadequate O<sub>2</sub> supply to the tissue, most probably due to a restriction of the microcirculation and thus of the O<sub>2</sub> availability to the cancer cells *in vivo*. As the tumors increase in size, this situation is significantly aggravated. Besides intratumor heterogeneities, there is a marked tumor-to-tumor variability, even if tumors of the same size, at the same growth site, and of the same cell line are compared. Evaluations of the vascular density in carcinomas of the uterine cervix are in accordance with the pO<sub>2</sub> data reported (91, 108, 109). In these studies the mean intercapillary distances (304 ± 30 μm) either were relatively independent of the clinical stage and histological grade (108) or revealed a

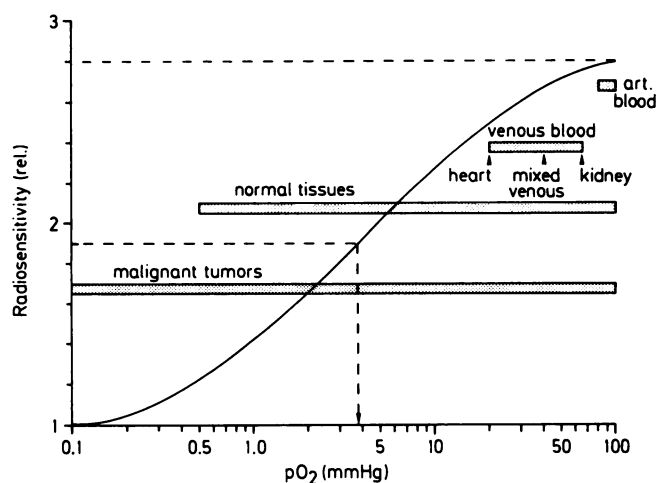


Fig. 5. Relative radiosensitivity as a function of O<sub>2</sub> partial pressure (pO<sub>2</sub>) in the cellular environment (schematic representation). Range of pO<sub>2</sub> values usually found in blood, normal tissues, and malignant tissues (shaded bars) and O<sub>2</sub> partial pressure at which the sensitizing effect is half-maximal (3–4 mm Hg) are indicated.

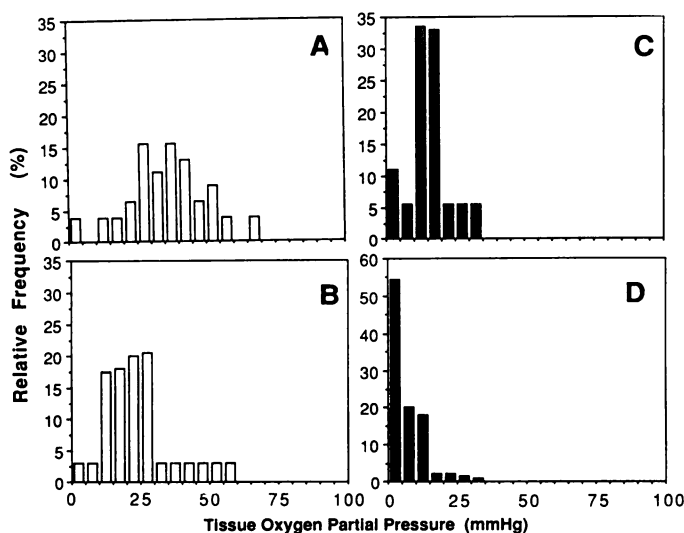


Fig. 6. pO<sub>2</sub> distribution in normal cervix mucosa (A) and in cervix cancers at different clinical stages. B, stage 0; C, stage I; D, stage II [pooled data are given (91, 101)].

gradual increase with advancing stage of the disease (91, 109).

**Oxyhemoglobin Saturation of Single RBC in Tumor Microvessels.** As already mentioned, characterization of the oxygen status is also possible using a cryospectrophotometric *ex vivo* technique which allows for the measurements of the HbO<sub>2</sub> saturation of individual RBC in tumor microvessels. HbO<sub>2</sub> cryospectrophotometry was introduced into experimental tumor biology by Vaupel *et al.* (60, 110–113). In recent reports, Rofstad *et al.* (114–116) have characterized the oxyhemoglobin saturation status of murine tumors and of xenografted human tumors (114, 116) using a similar technique. From all studies performed thus far using animal models there is clear indication that (a) the HbO<sub>2</sub> saturations were significantly lower in tumors than in normal host tissues, (b) HbO<sub>2</sub> values were gradually shifted towards lower values as the tumor volumes increase, (c) different tumor cell lines yield different oxygenation patterns (117), and (d) growth site is a relevant parameter governing tumor tissue oxygenation (111, 117). As was the case with the tumor tissue pO<sub>2</sub> distributions, this technique also revealed substantial intratumor heterogeneity and tumor-to-tumor variability.

Characterization of the oxygen status of human tumors *in situ* was also possible using this technique. As a typical example, in Fig. 7 the HbO<sub>2</sub> frequency distribution is shown for differentiated adenocarcinomas of the rectum and for the normal rectal mucosa (118). As a rule, the mean HbO<sub>2</sub> values observed in the tumors are distinctly lower than those found in the normal tissue at the site of tumor growth. The same holds for squamous cell carcinomas of the oral cavity (120). The medians of the HbO<sub>2</sub> frequency distributions of the normal oral mucosa and of the tumors decreased from 80 to 49 saturation % (see Fig. 7) and correlated with changes in vascular density.

Here again, in various malignant tumors considerable inter- and intraindividual differences were observed, even when tumors of the same clinical stage and grade were investigated. As a representative example for pronounced intratumor heterogeneities, the oxygenation status of a metastatic lesion of a small cell carcinoma of the lung in the humerus is depicted in Fig. 8. From the various distributions of measured HbO<sub>2</sub> data of individual RBC there is a clear indication for substantial heterogeneities in the oxygenation status among 4 different cryobiopsies of the same metastatic lesion. In addition, multimodal distributions in some cryobiopsies are indicative of heterogeneities in the oxygenation within an individual cryobiopsy (119). The HbO<sub>2</sub> data obtained for normal rectal mucosa and for adenocarcinomas of the rectum can be related to the respec-

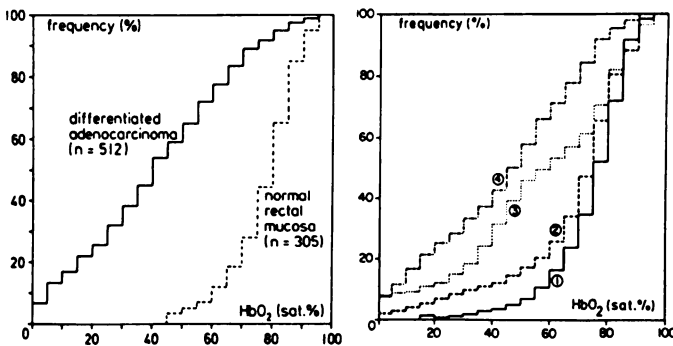


Fig. 7. *Left*, cumulative frequency distribution curves of HbO<sub>2</sub> of individual RBC within microvessels of the normal rectal mucosa and of differentiated adenocarcinomas of the rectum [*n* = number of HbO<sub>2</sub> measurements (118 and 119)]. *Right*, cumulative frequency distribution curves of HbO<sub>2</sub> values of the normal oral mucosa (Curve 1), of well vascularized tumors (Curve 2), of neoplasms with medium quality of vascularization (Curve 3), and of poorly vascularized cancers of the oral cavity (Curve 4) (119, 120).

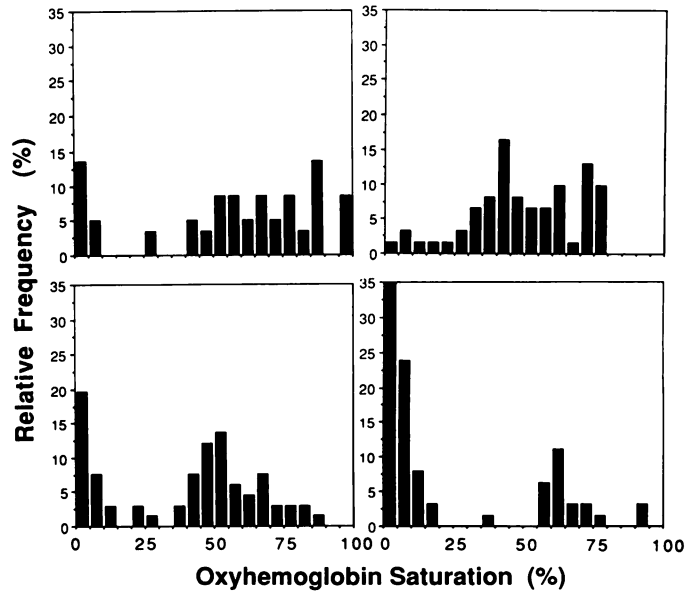


Fig. 8. Histograms of measured HbO<sub>2</sub> saturations of individual red blood cells within microvessels of 4 cryobiopsies taken from a metastatic lesion of a small cell carcinoma of the lung in the left humerus of a male patient.

tive vascularization. In the normal mucosa the vascular density was 2.5 times higher than in rectal cancers. In addition, the distribution of microvessels in the adenocarcinomas is very heterogeneous with considerable inter- and intratumor variations (121). In contrast, a regular vascular pattern exists in the normal mucosa.

Considering pooled data for the oxygen partial pressure distributions in various human malignancies and taking into account the available information on the HbO<sub>2</sub> saturation in human tumors there is experimental evidence for the existence of hypoxia in human tumors especially at advanced growth stages, *i.e.*, in bulky tumors. In the case of the oxyhemoglobin saturation measurements, hypoxia is to be expected in central portions of the intercapillary space if HbO<sub>2</sub> values fall below 30 saturation %. Both in diffusion-limited hypoxia (“chronic hypoxia”) and in ischemic hypoxia (“acute hypoxia”) O<sub>2</sub> deficiency starts to develop first in tissue areas far away from a tumor capillary and, most seriously, at the venous end of the microvessel.

**Nutrient Uptake Rates of Human Tumors *in Situ***

*Glucose Consumption*

Over 60 years ago, Warburg (70) studied the glucose turnover using tumor slices incubated aerobically and noted high rates of lactic acid production. From these experiments and others, an attitude regarding the high rate of aerobic glycolysis and lactate release became a biochemical “hallmark” of malignancies. Since that time, further insight into this aspect of tumor energy metabolism has been added including three different mechanisms of glucose turnover: glucose oxidation; aerobic glycolysis (breakdown of glucose to lactic acid in the presence of oxygen); and anaerobic glycolysis (breakdown of glucose to lactic acid in the absence of oxygen).

The investigation of Warburg’s hypothesis under *in vivo* conditions was permitted by the development of “tissue-isolated” tumor preparations using kidney, ovary, testis, or an inguinal fat pedicle as implantation sites (122–126). In these studies, blood flow, glucose uptake, and lactate production of

isotransplanted rat tumors were measured. Recently, the inguinal implantation site was used to study the turnover of glucose and other substrates like ketone bodies and amino acids (127–130).

As a rule, in these studies the glucose uptake rate was directly proportional to the glucose availability; *i.e.*, the glucose consumption was governed by tumor blood flow assuming constant arterial glucose concentrations during normoglycemia. These *in vivo* studies further revealed a deprivation of nutrients and an insufficient removal of metabolic waste products, predominantly lactic acid, causing tissue acidosis. Because blood flow through most of the isotransplanted tumors investigated was already compromised in small tumors and inadequacy in flow aggravated during tumor growth, weight-adjusted glucose uptake rates declined with enlarging tumor volume.

From studies using xenografted human tumors there is again evidence that the substrate supply and not the metabolic demand of the tumor cells limits the glucose uptake. This is probably due to the fact that even in high-flow tumors supply rates are not high enough to meet the demand of the cells. This finding infers steep concentration gradients for glucose in the extravascular space of human tumor xenografts (23, 131, 132). The capacity to consume glucose varied 4-fold between the different human cell lines. Due to an anisotropic flow distribution in individual tumors of one cell line, a heterogeneous glucose uptake rate must be expected within the tumor mass. As a rule, the amount of lactate released was linearly related to the amount of glucose consumed. Assuming steady state conditions and glucose to be the only substrate source of lactate, the glycolytic rate can be determined as the ratio of the lactate release and the glucose uptake. With this assumption, it was found that depending on the human cell line investigated, 40–85% of the glucose taken up can be released as lactate. These data represent average rates with substantially lower rates in small tumors and higher proportions in bulky malignancies (23, 132). In the xenograft studies, pH values in the tumor venous blood were close to arterial levels in tumors with high flow rates despite high lactate release rates. At perfusion rates <0.2 ml/g/min, tumor venous blood was acidic, and pH values as low as 7.1 occurred, indicating that tumor tissue acidosis mainly develops due to inadequate drainage through tumor tissue perfusion (132).

Using a vessel cannulation technique, Richtsmeier *et al.* (133) have measured arteriovenous concentration differences for glucose, lactic acid, and other substrates in head and neck cancers of patients. The mean arteriovenous metabolite concentration differences were 1.75 mM for glucose and –0.46 mM for lactate. The glucose utilization rate was 15%. Considering glucose as the only source for lactic acid production, the glycolytic rate (lactate release rate/glucose uptake rate) is estimated to be 13%. Assuming a mean blood flow for human head and neck tumors of 0.136 ml/g/min (51), the glucose uptake rate is 0.24  $\mu\text{mol/g/min}$ , and the lactate release rate is 0.06  $\mu\text{mol/g/min}$  (see Table 6). Since the mean shunt flow was 23% (range, 8–43%) in these studies (51), the “true” uptake or release rates may have been considerably higher.

To increase the understanding of human cancer metabolism, PET has been used successfully to measure regional glucose consumption. The positron-emitting radionuclides chosen to measure glucose utilization in tumors (mostly brain tumors) and normal brain were [ $^{18}\text{F}$ ]-2-deoxyglucose and [ $^{11}\text{C}$ ]-2-glucose, respectively. Tracer models involved in these studies, however, are still open to criticism especially when dealing with malignancies.

Several investigators attempted to characterize the glucose utilization of brain tumors (see Table 6). Di Chiro *et al.* (135) found a strong correlation between the glucose consumption rate and the grade of astrocytomas, with visual “hot spots” present in all high-grade tumors (grades III and IV) and only in a few low-grade lesions (grades I and II). The analysis of 100 patients revealed an average glucose uptake rate of grade I and II astrocytomas of  $0.21 \pm 0.10 \mu\text{mol/g/min}$ , compared to  $0.30 \pm 0.15 \mu\text{mol/g/min}$  in cases of grade III and  $0.41 \pm 0.20 \mu\text{mol/g/min}$  in verified cases of grade IV astrocytomas. However, for individual diagnosis, the absolute metabolic rate was found to be less useful than the visual appearance of the PET scan. In addition, these investigators found a regional depression of the glucose uptake in peritumoral regions. Seventeen patients with intracranial meningiomas were studied by Di Chiro *et al.* (134). In this investigation, the authors showed that the glucose-metabolic rates correlated with the tumor growth rate. They concluded that the glucose utilization rate appears to be at least as reliable as histological classification and other proposed criteria for predicting the therapeutic response and recurrence of intracranial meningiomas.

Similar correlations were found for the amino acid uptake of astrocytomas and the histological grading. In grade IV tumors the L-[ $^{11}\text{C}$ ]methionine uptake was twice the value found in grade II lesions (149). Using metabolic imaging of human soft tissue sarcomas by PET, again a good correlation was found between the glucose uptake rate and the histopathological grading [glucose uptake rate was increased 4-fold in grade III tumors compared to grade I malignancies (138)].

Patronas *et al.* (137) used the PET technique to evaluate a group of patients with proved high-grade gliomas to see if the data obtained had any prognostic value. In this study, radiation-induced tumor necrosis was associated with a reduced glucose utilization in the lesion, whereas in recurrent gliomas the glucose uptake was elevated. Similar differences were reported by Di Chiro *et al.* (134). These authors found a 2-fold higher glucose uptake rate in recurrent and/or regrowing meningiomas than in tumors that did not recur. On the average, glucose uptake of brain tumors was not significantly different from that obtained for the normal cerebral cortex (see Table 6). In lung cancers and soft tissue sarcomas, glucose utilization was 3–6 fold higher than in the normal tissues at the site of tumor growth, indicating a high glucose demand of malignancies with

Table 6 Glucose uptake rates ( $\dot{V}_{\text{Glu}}$ ) of human malignancies and of normal tissues (PET-derived data)

Tissue	$\dot{V}_{\text{Glu}}$ ( $\mu\text{mol/g/min}$ )	Refs.
Meningiomas	0.03–0.43	134
Astrocytomas		
Grades I–II	0.14–0.43	135, 136
Grades III–IV	0.12–0.88	137, 39
Soft tissue sarcomas	0.15–0.51	138
Lung cancers	0.11	139
Squamous cell carcinomas	0.24 <sup>a</sup>	133
Whole brain	0.30–0.40	140
Gray matter	0.25–0.51	141
White matter	0.08–0.28	142
Brain stem	0.18–0.28	143
Spinal cord	0.09	144–147
Lung parenchyma	0.017	139
Myocardium	0.6–1.5	148
Skeletal muscle (at rest)	0.05–0.07 <sup>b</sup>	

<sup>a</sup> Calculated uptake rate considering a mean blood flow of head and neck cancers of 0.136 ml/g/min (51).

<sup>b</sup> Uptake rate for quadriceps muscle in rodents (F. Kallinowski *et al.*, unpublished results).

an increase in the nonoxidative glucose metabolism (tumor cells are "avid" glucose consumers).

### Other Nutrients

Sauer *et al.* (129) have suggested that ketone bodies may be important fuels for tumor growth *in vivo* in fasted and semi-fasted animals. They found that both acetoacetate and  $\beta$ -hydroxybutyrate were utilized by isotransplanted rat tumors *in vivo* and that the uptake rates were directly proportional to the respective availabilities. Interestingly, in these experiments lactate was also utilized when arterial lactate levels exceeded 3 mM.

Ketone body metabolism has also been shown to be a qualitatively important feature in human breast cancer xenografts (132). Here again, the uptake rates were linearly related to the respective availabilities. The mean uptake of  $\beta$ -hydroxybutyrate was 3.5 nmol/g/min and that of acetoacetate was 2.6 nmol/g/min. At similar availabilities the uptake rates of the ketone bodies were comparable for the isografted rodent tumors and the xenografted human breast carcinomas. In the human tumor xenografts the  $\beta$ -hydroxybutyrate/acetoacetate ratio in the tumor venous blood rose with decreasing tumor blood flow (which occurred with increasing tumor volume) indicating a heavy reliance on anaerobic metabolic pathways, at advanced growth stages (132).

The first and only direct demonstration of ketone body uptake by human tumors *in vivo* was published by Richtsmeier *et al.* (133). In this study arteriovenous concentration differences for  $\beta$ -hydroxybutyrate and acetoacetate in head and neck cancers were measured. The respective mean concentration differences were 0.07 mM for  $\beta$ -hydroxybutyrate, and 0.09 mM for acetoacetate. All tumors studied took up the ketone bodies but in varying amounts indicating metabolic heterogeneity between the tumors. The utilization was 14% for  $\beta$ -hydroxybutyrate and 38% for acetoacetate. Assuming a mean blood flow rate of head and neck cancers of 0.136 ml/g/min (51) the respective uptake rates were 9.5 nmol/g/min for  $\beta$ -hydroxybutyrate and 12.2 nmol/g/min for acetoacetate. Comparable uptake rates were found for xenografted human breast cancers (132). Ketone body uptake by human tumors appears to be proportional to the availability. It seems reasonable to assume that the carbons of the ketone bodies are used for both energy metabolism and macromolecule synthesis in the squamous cell carcinomas studied.

Considerable evidence has accumulated indicating L-glutamine as a major substrate for the energy metabolism of rapidly growing tumor cells *in vitro*. Since oxygen is necessary for the oxidative breakdown of glutamine to pyruvate, an adequate oxygen supply to cancer cells during glutaminolysis is a prerequisite. Under *in vivo* conditions, however, hypoxia is a common feature in poorly vascularized malignancies. Considering this oxygen supply pattern, it may be postulated that glutamine can be a significant substrate for cancer cells only in the immediate neighborhood of nutritive tumor vessels and that due to the heterogeneous oxygenation of human tumors *in vivo*, glutaminolysis may also be heterogeneously distributed within the tumor mass (for a detailed discussion see Ref. 150).

### Metabolic Imaging of Human Tumors on a Microscopic Level

A method has been developed for metabolic imaging on a microscopic level in tumor tissues (151). This technique makes possible the determination of the spatial distribution of glucose,

lactate, and ATP in absolute terms at similar locations within tumors. The substrate distributions are registered using bioluminescence reactions in serial cryostat sections from tissue biopsies. The light emission is measured directly by a special imaging photon counting system allowing on-line image analysis. Thus far, this technique has been applied to human breast cancer xenografts and to primary adenocarcinomas of the rectum.

Preliminary data obtained indicate that heterogeneities in the substrate distributions measured are much more pronounced in tumors than in normal tissue (*e.g.*, resting skeletal muscle). There was no obvious correlation between glucose, lactate, and ATP levels measured at similar locations within the tissue (for further details see Ref. 151).

Biopsies were taken from human breast cancers xenografted into immunodeficient rats (132) and from untreated rectal carcinomas with special, cooled tongs and immediately dropped into liquid nitrogen (within 1 s). For measurement of the distributions of ATP, glucose, and lactate levels in these biopsies, the frozen tissue samples were cut into 20- $\mu$ m sections at  $-25^{\circ}\text{C}$ . The cryostat sections were then placed on coverglasses, freeze-dried, and except for the glucose measurements, heat inactivated. Afterwards, these sections were covered with 60- $\mu$ m cryostat sections of a frozen cocktail of enzymes that link the substrate of interest to the bioluminescence of luciferase. Upon thawing the sandwich of sections, the enzymes diffused into the tissue section, thus initiating the bioluminescence reaction (photoemission) which was registered by film exposure. The absorbance of the exposed film was then evaluated by microdensitometry and image analysis.

The spatial distribution of ATP in a section through a human breast cancer xenograft is shown in Fig. 9B. Although the data are plotted in relative units, they clearly illustrate pronounced heterogeneities in the ATP levels within these tumors. Microregions with very low ATP concentrations (yellow areas) are randomly distributed between areas with higher concentrations (green and red areas) in this section. The shape of the ATP distribution was highly reproducible between adjacent tissue sections. In general, the average ATP concentrations in those tumors were substantially lower (approximately 1 mM) than in normal skeletal muscle (as shown in Fig. 9A). ATP concentrations in skeletal muscle were not only distinctly higher (approximately 5–6 mM) but also more evenly distributed, although some heterogeneities were also present even in this normal tissue.

### Tumor pH

Rapidly growing tumor cells usually have a high metabolic rate which often cannot be adequately met by the nutrient supply under *in vivo* conditions. Carbon used for energy metabolism is derived from several sources (*e.g.*, glucose, amino and free fatty acids, ketone bodies, and even lactate when supplied in excess). During aerobic and/or anaerobic glycolysis, glutaminolysis, and ATP hydrolysis, hydrogen ions are formed which are actively transported outside the cell. Via the interstitial space the  $\text{H}^+$  ions finally reach the blood vessels and are removed from the tissue thereafter by convective transport. If a high glycolytic rate and a high lactic acid production coincide with an insufficient drainage by convective and/or diffusive transport,  $\text{H}^+$  ions accumulate in the respective tissue. As a result, pH is shifted to more acidic values, especially in bulky and/or low-flow tumors (23). If microcirculatory inadequacy is combined with functional heterogeneity, pH variability becomes

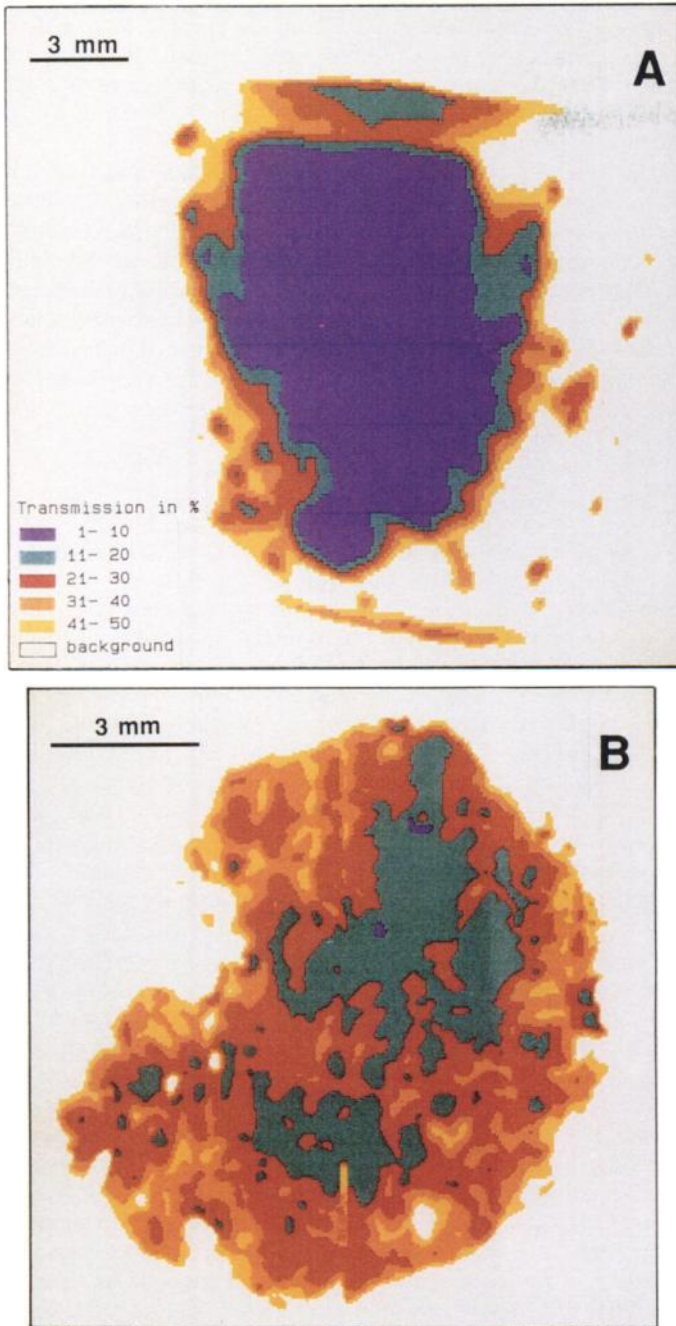


Fig. 9. Regional distribution of ATP concentrations in resting skeletal muscle (A) and in a human breast cancer xenograft (B). High ATP levels are present in the violet areas, low concentrations in the yellow regions. On the average, ATP levels in tumors are distinctly lower than in normal tissues and substantially more anisotropic.

a common feature both within a tumor and between tumors. A basic prerequisite for the development of acidosis, however, is that glucose is available to hypoxic cancer cells. Since the diffusion distance for glucose is larger than that for  $O_2$ , this prerequisite is usually met. In a recent paper, Kallinowski *et al.* (150) have estimated that this holds true for xenografted human breast cancers; *i.e.*, hypoxic tumor cells far away from the supplying vessel can still cleave glucose to lactic acid. Therefore, it is not surprising that inverse correlations between the lactic acid content and the interstitial pH have been found in tumors (152–154).

Much work has been done on the effect of acidosis upon cells in tissue culture and in animal tumor systems (for a review see Ref. 12). Low pH has been shown to inhibit cell proliferation,

DNA synthesis, and glycolysis. A shift of cells to  $G_1$  and  $G_0$  in the cell cycle has been described. In addition, a loss in transplantability and an enhancement of metastasis formation have been found under experimental conditions. Acidosis can decrease the radiosensitivity of mammalian cells, modulate the cytotoxicity of certain anticancer drugs, influence the thermal radiosensitization, enhance the cell killing effect of heat, and inhibit the development of thermotolerance. Modification of baseline pH in tumors is possible by administration of glucose and upon tumor treatment, especially hyperthermia at temperatures above  $42^\circ C$  and treatment times exceeding 15 min.

The pH of human tumor tissues has been measured by a variety of techniques. The most traditional technique is the use of pH-sensitive electrodes with tip diameters ranging from  $0.5 \mu m$  to 2 mm. This method has the disadvantage that it is invasive and, therefore, that large electrodes can affect tumor microcirculation and thus the cellular metabolic microenvironment. Whereas the microelectrode technique allows for the description of the pH distribution in microareas of the tumors, miniaturized electrodes can register integrated pH values only from a relatively large tumor volume. Thus far, there are no significant differences between the average tumor pH values obtained with micro- or with minielectrodes. Since these measurements are based on the potentiometric technique, in the following pH data obtained with electrodes are designated as  $pH_{POT}$ . What is actually measured by electrodes is generally accepted to mainly represent the hydrogen ion activity<sup>6</sup> rather than the  $H^+$  concentration. pH values obtained with microelectrode measurements are a composite pH with contributions from the interstitial and intravascular pH expected to be at least 50% (66). In contrast to the electrode measurements,  $pH_{PET}$  and  $pH_{NMR}$  are largely dependent upon the pH of the intracellular space.

#### $pH_{POT}$

Compared to the values in normal tissues, tumor pH distributions obtained in animal studies are generally shifted to more acidic values ( $\Delta pH = 0.3$ – $0.5$  unit). pH values in spontaneous rat tumors were not significantly different from those found in isotransplanted malignancies (7). There is a trend towards more acidic pH values as the tumor mass enlarges with a broad range of pH values determined. This wide range most probably is due to intratumor heterogeneities, to tumor-to-tumor variations, and possibly to variations between different tumor pathologies (for reviews, see Refs. 7 and 12).

The wide range of pH values that have been determined in human tumors using electrode measurements is shown in Fig. 9. Pooled data are given for primary brain tumors and brain metastases (155), malignant melanomas (156, 157), sarcomas (157, 158), breast cancer (12, 159), squamous cell carcinomas, and adenocarcinomas (150). The measurements of Inch (160), Meyer *et al.* (161), Millet (162), Naeslund and Swenson (163), and Okuneff (164) cannot be regarded as being relevant since they are “burdened” with methodological problems.

Whereas most human tumors exhibit pH values between 6.15 and 7.40 (the latter value representing the mean pH of arterial

<sup>6</sup> The definition of the activity  $a$  of a component  $i$  is contained in the relationship

$$\mu_i = \mu_i^\circ + RT \ln a_i$$

where  $R$  is the gas constant (per mol),  $T$  is the absolute temperature,  $\mu_i$  is the chemical potential of the component, and  $\mu_i^\circ$  is the chemical potential in the standard state.

blood), normal tissues usually have pH values between 7.0 and 7.4. There are only a few tumors reported (astrocytomas and squamous cell carcinomas) with pH values <6.0. The pH data obtained in brain tumors and melanomas were significantly lower than those in normal cerebral gray matter and in the skin, respectively ( $P < 0.001$ ).

In addition to human tumor pH values, a summary of normal tissue pH values is given in Fig. 10. Pooled data are compiled for resting skeletal muscle (157, 165–170), skin (156, 157, 171–174), brain (155), arterial blood (25), and RBC [(175) pH variations in RBC are in part due to varying oxyhemoglobin saturations and the use of freeze-thaw processes].

In mammary carcinomas and in skin, pH values higher than those in arterial blood are reported. This may at least be partly due to temperatures <37°C and to a CO<sub>2</sub> loss from superficial tissue layers into the surroundings. In the case of the breast carcinomas, it must also be taken into account that in bulky tumors with gross, long-standing necrosis the mean tissue pH can be distinctly higher than in arterial blood. This “alkalotic” pH shift is caused by a cessation of all H<sup>+</sup>-producing metabolic processes and a binding of protons during protein denaturation.

*pH<sub>PET</sub>*

Rottenberg *et al.* (176) have developed a method for measuring tissue pH with [<sup>11</sup>C]DMO and positron emission tomography. DMO is a weak acid with a pK<sub>a</sub> of 6.12. If it is assumed that the extracellular and intracellular concentration of the non-ionized portion of the acid (*i.e.*, the diffusible form) are equal, then the tissue pH can be calculated using the Henderson-Hasselbalch equation if the local [<sup>11</sup>C]DMO concentration is

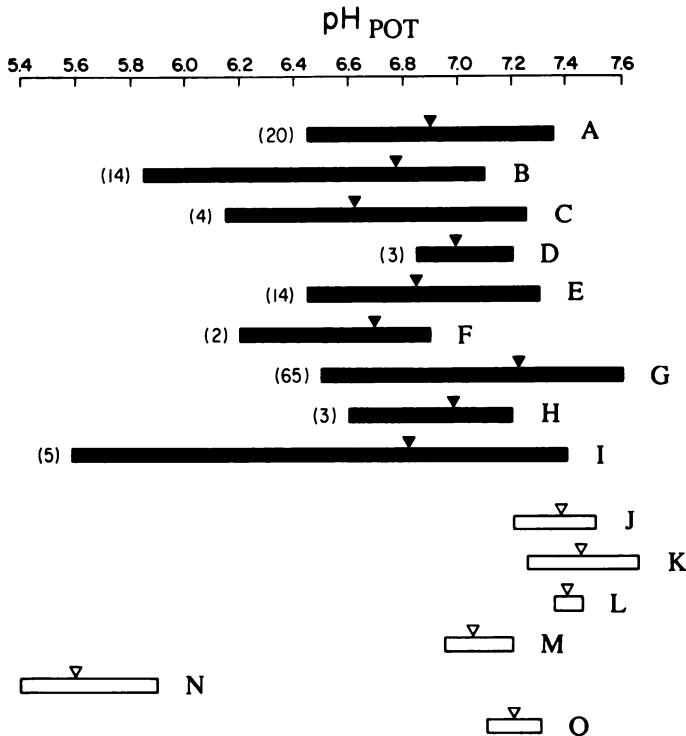


Fig. 10. Compilation of pooled pH values measured with pH-sensitive electrodes (pH<sub>POT</sub>) in human tumors (■), and in normal tissues (□). Arrowheads, respective mean values; numbers in parentheses, number of tumors investigated. A, glioblastomas; B, astrocytomas; C, meningiomas; D, brain metastases; E, malignant melanomas; F, sarcomas; G, mammary carcinomas; H, adenocarcinomas; I, squamous cell carcinomas; J, resting skeletal muscle; K, skin (at 37°C); L, arterial blood; M, brain; N, skin (surface); O, erythrocyte (the respective references are given in the text).

measured quantitatively with PET (177). The measured tissue pH is a composite value of intracellular (pH<sub>i</sub>) and the extracellular pH. Calculation of pH<sub>i</sub> is possible if measurements of total tissue water content and of the fractional volume of the extracellular water are known (178).

Human PET studies with [<sup>11</sup>C]DMO are rare and thus far little patient data are available, although this technique represents an interesting concept for further testing in human studies. Recent investigations have revealed generally more alkaline values in brain tumors than in normal gray or white matter (see Table 7). As discussed by Junck *et al.* (181), differences in the size of the interstitial spaces of tumors and normal brain tissue might be responsible for the relative alkalinity of the tumors. This hypothesis, however, must be tested in further experiments (for a detailed discussion see “pH<sub>NMR</sub>”).

*pH<sub>NMR</sub>*

Magnetic resonance spectroscopy of human tumors and its potential *in vivo* clinical applications have been reviewed recently (182, 183). <sup>31</sup>P nuclear magnetic resonance spectroscopy is able to provide important biochemical information in living tissues, especially of high-energy phosphate and (membrane) phospholipid metabolism. Because *in vivo* <sup>31</sup>P NMR observes the unperturbed biochemical processes at the molecular level, the effect of cancer treatments would most likely be revealed in the spectra earlier than other traditional techniques, such as biopsies or other laboratory analyses. In addition, because the nuclear magnetic resonance spectroscopy technique is noninvasive, nonperturbing, and painless, it allows the patient to be repeatedly monitored throughout the course of treatments (184).

*In vivo* <sup>31</sup>P NMR spectroscopy has been used to monitor the energy metabolism of human tumors since 1983 (185). From the studies available, information is provided that may be useful for diagnostic informations or beneficial in clinical treatment of cancer. Furthermore, there are hints that serial monitoring of tumor response can assist in optimizing the timing of treatments. If <sup>31</sup>P NMR spectra from normal tissues (*e.g.*, skeletal muscle or parenchymal breast) are compared with their malignant counterparts, abnormally high concentrations of PME, phosphodiesteres, and P<sub>i</sub> and low PCr levels are characteristic for the latter. Unlikely many isotransplanted murine tumors and human tumor xenografts, human malignancies have relatively lower P<sub>i</sub> levels and somewhat higher NTP signals. This may be an indication that the hypoxic cell fraction in human neoplasms is smaller than in some rapidly growing rodent tumors. As a rule, in malignant tumors the NTP/P<sub>i</sub> ratio is lower compared with that in normal or uninvolved tissue from the same patient. In tumors of mesenchymal origin and in brain tumors, the PCr/NTP and the NTP/P<sub>i</sub> ratios are both reduced compared to muscle and brain, respectively. This is consistent

Table 7 Tissue pH values in normal brain and in brain tumors (measurements using <sup>11</sup>C and positron emission tomography in patients)

Tissue	Method	Tissue pH	Refs.
Whole brain	<sup>11</sup> CO <sub>2</sub> (continuous inhalation)	6.96–7.05	179
Whole brain	[ <sup>11</sup> C]DMO	6.75–7.07 <sup>a</sup>	178
Gray matter		6.74–7.09	180
White matter		6.77–7.03	
Cerebellum		7.03–7.05	176
Meningiomas	[ <sup>11</sup> C]DMO	7.23–7.26	176, 180
Gliomas		7.15–7.22	
Brain metastases		6.91–7.10	

<sup>a</sup> Intracellular pH.

with a more anaerobic tumor metabolism (183) and a depletion of energy stores.

pH values as measured by  $^{31}\text{P}$  nuclear magnetic resonance ( $^{31}\text{P}$  NMR) spectroscopy are best considered a composite pH with contributions from intracellular pH expected to be at least 85% of the total (186). In general, the PCr to  $\text{P}_i$  chemical shift is used to estimate the apparent intracellular pH in the tissues of interest (187). In the absence of a sharp PCr resonance, the  $\alpha$ -NTP resonance which is also pH insensitive can serve as a chemical shift reference, enabling pH determinations of similar accuracy.

Pooled pH data obtained from  $^{31}\text{P}$  NMR measurements are shown in Fig. 11. Values are given for various sarcomas (185, 188–190), squamous cell carcinomas (189–192), breast cancer (193, 194), brain tumors (191, 195–199), non-Hodgkin's lymphomas (184, 197, 200), miscellaneous malignancies (201), skeletal muscle (185, 188–190, 201–206), brain (191, 195, 197, 199, 201, 207, 208), liver (191, 209), heart (210), erythrocytes (211, 212), and lymphocytes (213). From the data available thus far there is clear evidence that the  $\text{pH}_{\text{NMR}}$  values for brain tumors are significantly higher than those obtained for normal brain structures. This finding is in accordance with pH data derived from PET studies. Furthermore,  $\text{pH}_{\text{NMR}}$  values in sarcomas tend to be somewhat higher than those for resting skeletal muscle. pH differences seen between normal tissues (skeletal muscle, brain) and malignancies (brain tumors, sarcomas) are on the order of 0.1 pH unit. The exact mechanisms causing these (unexpected) pH differences are unknown at present.

As a rule, intracellular pH is normally maintained above the equilibrium pH by active net proton transport into the extracellular space (214). According to the report of Arnold *et al.* (195) the more alkaline pH in brain tumors and sarcomas compared to the respective normal tissues may be due to an enhanced active  $\text{H}^+$  transport into the extracellular compartment, an increased cellular buffering capacity, a net change in cellular strong organic acid concentration (*e.g.*, lactic acid), and/or an increase in the equilibrium potential for  $\text{H}^+$  ions.

At the moment the most convincing theory explaining the progressive alkalinization of (certain) tumor cells is based on a loss of membrane potential secondary to a redistribution of  $\text{K}^+$

and other ions. As the membrane potential becomes more positive than the equilibrium potential for  $\text{H}^+$  ions (approximately  $-24$  mV, see Ref. 195), this mechanism can result in a passive hydrogen ion efflux from the cell yielding intracellular alkalinization.

In a very recent study, Ng *et al.* (192) have observed normal and alkaline pH values in 34 of 35 superficial tumors examined, thus confirming earlier results on brain tumors and sarcomas. In the latter investigation, pH ranged from 6.90 to 7.60 (mean pH, 7.22) in squamous cell carcinomas of the head and neck (lymph nodes), from 7.21 to 7.60 (mean pH, 7.34) in non-Hodgkin's lymphomas, from 7.09 to 7.67 (mean pH, 7.36) in Hodgkin's lymphomas, and from 7.40 to 7.70 (mean pH, 7.57) in breast cancer.

#### Acknowledgments

The authors would like to thank Drs. R. K. Jain and J. Folkman for their encouragement to write this review. Furthermore, we would like to acknowledge the skillful assistance of Claudia Zanker in typing this manuscript.

#### REFERENCES

- Vaupel, P., and Mueller-Klieser, W. Interstitieller Raum und Mikromilieue in malignen Tumoren. *Progr. Appl. Microcirc.*, 2: 78–90, 1983.
- Vaupel, P., and Kallinowski, F. Microcirculation and metabolic micromilieue in malignant tumors. *Funktionsanal. Biol. Syst.*, 18: 265–271, 1988.
- Sartorelli, A. C. Therapeutic attack of hypoxic cells of solid tumors: presidential address. *Cancer Res.*, 48: 775–778, 1988.
- Sutherland, R. M. Cell and environment interactions in tumor microregions. The multicell spheroid model. *Science (Wash. DC)*, 240: 177–184, 1988.
- Mueller-Klieser, W. F., Walenta, S. M., Kallinowski, F., and Vaupel, P. Tumor physiology and cellular microenvironments. *In: J. D. Chapman, L. J. Peters, and H. R. Withers (eds.), Prediction of Tumor Treatment Response*, pp. 265–276. Elmsford, NY: Pergamon Press, 1989.
- Jain, R. K., and Ward-Hartley, K. Tumor blood flow—characterization, modifications and role in hyperthermia. *IEEE Trans. Sonics Ultrasonics, SU-31*: 504–526, 1984.
- Kallinowski, F., and Vaupel, P. pH distributions in spontaneous and iso-transplanted rat tumours. *Br. J. Cancer*, 58: 314–321, 1988.
- Song, C. W. Effect of local hyperthermia on blood flow and microenvironment. *Cancer Res. (Suppl.)*, 44: 4721s–4730s, 1984.
- Vaupel, P. Pathophysiologie der Durchblutung maligner Tumoren. *Funktionsanal. Biol. Syst.*, 8: 155–170, 1982.
- Vaupel, P., and Kallinowski, F. Physiological effects of hyperthermia. *Recent Results Cancer Res.*, 104: 71–109, 1987.
- Vaupel, P., Frinak, S., and Bicher, H. I. Heterogeneous oxygen partial pressure and pH distribution in C3H mouse mammary adenocarcinoma. *Cancer Res.*, 41: 2008–2013, 1981.
- Wike-Hooley, J. L., Haveman, J., and Reinhold, H. S. The relevance of tumour pH to the treatment of malignant disease. *Radiother. Oncol.*, 2: 343–366, 1984.
- Peterson, H.-I. (ed.). *Tumor Blood Circulation: Angiogenesis, Vascular Morphology and Blood Flow of Experimental and Human Tumors*. Boca Raton, FL: CRC Press, 1979.
- Shubik, P. Vascularization of tumors: a review. *J. Cancer Res. Clin. Oncol.*, 103: 211–226, 1982.
- Vaupel, P., and Hammersen, F. *Mikrozirkulation in malignen Tumoren. Progress in Applied Microcirculation*, Vol. 2. Basel: S. Karger AG, 1983.
- Grunt, T. W., Lametschwandner, A., and Staindl, O. The vascular pattern of basal cell tumors: light microscopy and scanning electron microscopic study on vascular corrosion casts. *Microvasc. Res.*, 29: 371–386, 1985.
- Reinhold, H. S., and van den Berg-Blok, A. Vascularization of experimental tumours. *CIBA Found. Symp.* 100: 100–110, 1983.
- Vaupel, P., and Gabbert, H. Evidence for and against a tumor type-specific vascularity. *Strahlenther. Oncol.*, 162: 633–638, 1986.
- Jain, R. K. Determinants of tumor blood flow: a review. *Cancer Res.*, 48: 2641–2658, 1988.
- Sevick, E. M., and Jain, R. K. Geometric resistance to blood flow in solid tumors perfused *ex vivo*: effects of tumor size and perfusion pressure. *Cancer Res.*, 49: 3506–3512, 1989.
- Sevick, E. M., and Jain, R. K. Viscous resistance to blood flow in solid tumors: effect of hematocrit on intratumor blood viscosity. *Cancer Res.*, 49: 3513–3519, 1989.
- Vaupel, P., Fortmeyer, H. P., Runkel, S., and Kallinowski, F. Blood flow, oxygen consumption and tissue oxygenation of human breast cancer xenografts in nude rats. *Cancer Res.*, 47: 3496–3503, 1987.

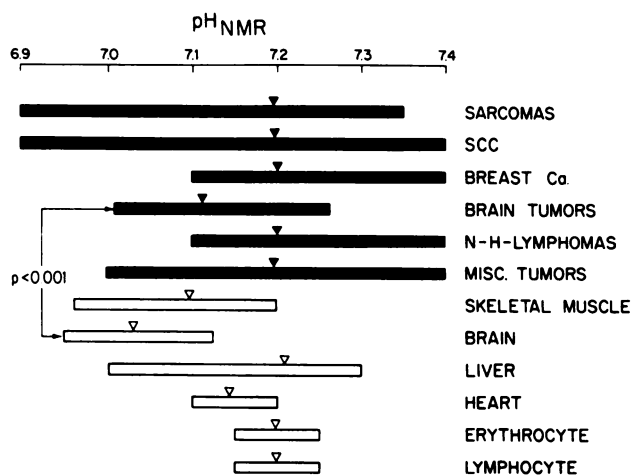


Fig. 11. Pooled pH data obtained from  $^{31}\text{P}$  NMR spectroscopy ( $\text{pH}_{\text{NMR}}$ ) performed on various human malignancies (■) and on normal organs (□): sarcomas, squamous cell carcinomas (SCC) (one tumor at  $\text{pH} \geq 7.6$  not listed), breast cancer (Ca.) (one tumor at  $\text{pH} \geq 7.6$  not listed), brain tumors, non-Hodgkin's lymphomas (one tumor at  $\text{pH} \geq 7.6$  not listed), miscellaneous tumors, resting skeletal muscle, brain, liver, heart, erythrocytes, lymphocytes. Arrowheads, respective mean pH values (the respective references are given in the text).

23. Kallinowski, F., Schlenger, K. H., Runkel, S., Kloes, M., Stohrer, M., Okunieff, P., and Vaupel, P. Blood flow, metabolism, cellular microenvironment, and growth rate of human tumor xenografts. *Cancer Res.*, **49**: 3759-3764, 1989.
24. Warnke, P. C., Friedman, H. S., Bigner, D. D., and Groothuis, D. R. Simultaneous measurements of blood flow and blood-to-tissue transport in xenotransplanted medulloblastomas. *Cancer Res.*, **47**: 1687-1690, 1987.
25. Thews, G., and Vaupel, P. *Autonomic Functions in Human Physiology*. Berlin: Springer-Verlag, 1985.
26. Shibata, H. R., and MacLean, L. D. Blood flow in tumors. *Progr. Clin. Cancer.*, **2**: 33-47, 1966.
27. Beaney, R. P. Positron emission tomography in the study of human tumors. *Semin. Nucl. Med.*, **14**: 324-341, 1984.
28. Beaney, R. P., Brooks, D. J., Leenders, K. L., Thomas, D. G. T., Jones, T., and Halnan, K. Blood flow and oxygen utilisation in the contralateral cerebral cortex of patients with untreated intracranial tumours as studied by positron emission tomography, with observations on the effects of decompressive surgery. *J. Neurol. Neurosurg. Psychol.*, **48**: 310-319, 1985.
29. Brooks, D. J., Beaney, R. P., Lammertsma, A. A., Turton, D. R., Marshall, J., Thomas, D. G. T., and Jones, T. Studies on regional cerebral haematocrit and blood flow in patients with cerebral tumours using positron emission tomography. *Microvasc. Res.*, **31**: 267-276, 1986.
30. Capon, A. Utilisation d'une méthode à thermodiffusion pour l'évaluation du débit sanguin dans les tumeurs cérébrales. *Acta Clin. Belg.*, **25**: 174-178, 1970.
31. Cronqvist, S., Ingvar, D. H., and Lassen, N. A. Quantitative measurements of regional cerebral blood flow related to neuroradiological findings. *Acta Radiol. Diagn.*, **5**: 760-766, 1966.
32. Reinhold, H. S. Physiological effects of hyperthermia. *Recent Results Cancer Res.*, **107**: 32-43, 1988.
33. Ito, M., Lammertsma, A. A., Wise, R. J. S., Bernardi, S., Frackowiak, R. S. J., Heather, J. D., McKenzie, C. G., Thomas, D. G. T., and Jones, T. Measurement of regional cerebral blood flow and oxygen utilisation in patients with cerebral tumours using <sup>15</sup>O and positron emission tomography: analytical techniques and preliminary results. *Neuroradiology*, **23**: 63-74, 1982.
34. Lammertsma, A. A. Positron emission tomography and *in vivo* measurements of tumour perfusion and oxygen utilisation. *Cancer Metastasis Rev.*, **6**: 521-539, 1987.
35. Lammertsma, A. A., Wise, R. J. S., and Jones, T. *In vivo* measurements of regional cerebral blood flow and blood volume in patients with brain tumours using positron emission tomography. *Acta Neurochir.*, **69**: 5-13, 1983.
36. Lammertsma, A. A., Wise, R. J. S., and Jones, T. Regional cerebral blood flow and oxygen utilisation in edema associated with cerebral tumours. *In: K. G. Go, and A. Baethmann (eds.), Recent Progress in the Study and Therapy of Brain Edema*, pp. 331-344. New York: Plenum Publishing Corp., 1984.
37. Lammertsma, A. A., Wise, R. J. S., Cox, T. C. S., Thomas, D. G. T., and Jones, T. Measurement of blood flow, oxygen utilization, oxygen extraction ratio, and fractional blood volume in human brain tumours and surrounding oedematous tissue. *Br. J. Radiol.*, **58**: 725-734, 1985.
38. Olesen, J., and Paulson, O. B. The effect of intra-arterial papaverine on the regional cerebral blood flow in patients with stroke or intracranial tumor. *Stroke*, **2**: 148-159, 1971.
39. Rhodes, C. G., Wise, R. J. S., Gibbs, J. M., Frackowiack, R. S. J., Hatazawa, J., Palmer, A. J., Thomas, D. G. T., and Jones, T. *In vivo* disturbance of the oxidative metabolism of glucose in human cerebral gliomas. *Ann. Neurol.*, **14**: 614-626, 1983.
40. Beaney, R. P., Lammertsma, A. A., Jones, T., McKenzie, C. G., and Halnan, K. E. Positron emission tomography for *in-vivo* measurements of regional blood flow, oxygen utilisation, and blood volume in patients with breast carcinoma. *Lancet*, **1**: 131-134, 1984.
41. Johnson, R. A thermodynamic method for investigation of radiation induced changes in the microcirculation of human tumors. *Int. J. Radiat. Oncol. Biol. Phys.*, **1**: 659-670, 1976.
42. Lahtinen, T., Karjalainen, P., and Alhave, E. Measurement of blood flow with a <sup>133</sup>Xe washout method. *Eur. J. Nucl. Med.*, **4**: 435-439, 1979.
43. Mäntylä, M., Heikkonen, J., and Perkkio, J. Regional blood flow in human tumours measured with argon, krypton and xenon. *Br. J. Radiol.*, **61**: 379-382, 1988.
44. Samulski, T. V., Fessenden, P., Valdagni, R., and Kapp, D. S. Correlations of thermal washout rate, steady state temperatures, and tissue type in deep seated recurrent or metastatic tumours. *Int. J. Radiat. Oncol. Biol. Phys.*, **13**: 907-916, 1987.
45. Taylor, I., Bennett, R., and Sherriff, S. The blood supply of colorectal liver metastases. *Br. J. Cancer*, **39**: 749-756, 1979.
46. Wartnaby, K. M., Bouchier, I. A. D., Pope, C. E., and Sherlock, S. Hepatic blood flow in patients with tumors of the liver. *Gastroenterology*, **44**: 733-739, 1963.
47. Mäntylä, M. J. Regional blood flow in human tumors. *Cancer Res.*, **39**: 2304-2306, 1979.
48. Mäntylä, M. J., Toivanen, J. T., Pitkänen, M. A., and Rekonen, A. H. Radiation-induced changes in regional blood flow in human tumors. *Int. J. Radiat. Oncol. Biol. Phys.*, **8**: 1711-1717, 1982.
49. Nyström, C., Forssman, L., and Roos, B. Myometrial blood flow studies in carcinoma of the corpus uteri. *Acta Radiol. Ther.*, **8**: 193-198, 1969.
50. Waterman, F. M., Nerlinger, R. E., Moylan, D. J., and Leeper, D. B. Response of human tumor blood flow to local hyperthermia. *Int. J. Radiat. Oncol. Biol. Phys.*, **13**: 75-82, 1987.
51. Wheeler, R. H., Ziessman, H. A., Medvec, B. R., Juni, J. E., Thrall, J. H., Keyes, J. W., Pitt, S. R., and Baker, S. R. Tumor blood flow and systemic shunting in patients receiving intraarterial chemotherapy for head and neck cancer. *Cancer Res.*, **46**: 4200-4204, 1986.
52. Plengvanit, K., Suwanak, R., Chearani, O., Intrasupt, S., Sutayavanich, S., Kalayisir, C., and Viranuvatti, V. Regional hepatic blood flow studied by intrahepatic injection of <sup>133</sup>Xenon in normals and in patients with primary carcinoma of the liver, with particular reference to the effect of hepatic artery ligation. *Aust. NZ J. Med.*, **1**: 44-48, 1972.
53. Touloukian, R. J., Rickert, R. R., Lange, R. C., and Spencer, R. P. The micro-vascular circulation of lymphangiomas: a study of Xe<sup>133</sup> clearance and pathology. *Pediatrics*, **48**: 36-40, 1971.
54. Tanaka, Y. Regional tumor blood flow and radiosensitivity. *In: T. Sugahara, L. Revesz, and O. Scott (eds.), Fraction Size in Radiobiology and Radiotherapy*, pp. 13-26. Munich: Urban & Schwarzenberg, 1974.
55. Bru, A., Combes, P. F., Douchez, J., Lucot, H., and Ribot, J. F. Estimation de l'activité circulatoire à l'intérieur des tumeurs ganglionnaires malignes par la mesure du taux déposition du xenon-133. *In: IAEA Proceedings, Dynamic Studies with Radioisotopes in Medicine*, pp. 633-642. Rotterdam: 1970.
56. Lebrun-Grandié, P., Baron, J.-G., Soussaline, F., and Loch'h, C. Coupling between regional blood flow and oxygen utilization in the normal human brain. *Arch. Neurol.*, **40**: 230-236, 1983.
57. Powers, W. J., Grubb, R. L., and Raichle, M. E. Physiological response to focal cerebral ischemia in humans. *Ann. Neurol.*, **16**: 546-552, 1984.
58. Selwyn, A. P., Shea, M. J., Foale, R., Deanfield, J. E., Wilson, R., de Landsheere, C. M., Turton, D. L., Brady, F., Pike, V. W., and Brookes, D. I. Regional myocardial and organ blood flow after myocardial infarction: application of the microsphere principle in man. *Circulation*, **73**: 433-443, 1986.
59. Endrich, B., Hammersen, F., Goetz, A., and Messmer, K. Microcirculatory blood flow, capillary morphology, and local oxygen pressure of the hamster amelanotic melanoma A-MEL-3. *J. Natl. Cancer Inst.*, **68**: 475-485, 1982.
60. Vaupel, P., Grunewald, W. A., Manz, R., and Sowa, W. Intracapillary HbO<sub>2</sub> saturation in tumor tissue of DS-carcinoma during normoxia. *Adv. Exp. Med. Biol.*, **94**: 367-375, 1978.
61. Weiss, L., Hultborn, R., and Tveit, E. Blood flow characteristics in induced rat mammary neoplasia. *Microvasc. Res.*, **17**: 119, 1979.
62. Groebe, K., and Vaupel, P. Evaluation of oxygen diffusion distances in human breast cancer xenografts using tumor-specific *in vivo*-data: role of various mechanisms in the development of tumor hypoxia. *Int. J. Radiat. Oncol. Biol. Phys.*, **15**: 691-697, 1988.
63. Vaupel, P. Interrelationship between mean arterial blood pressure, blood flow, and vascular resistance in solid tumor tissue of DS-carcinoma. *Experientia (Basel)*, **31**: 587-589, 1975.
64. Peterson, H.-I. Innervation von Tumorgefäßen, Einfluss vasoaktiver Substanzen und Regulation der Tumordurchblutung. *Progr. Appl. Microcirc.*, **2**: 69-77, 1983.
65. Jirtle, R. L. Chemical modification of tumour blood flow. *Int. J. Hyperthermia*, **4**: 355-371, 1988.
66. Vaupel, P. Durchblutung, Oxygenierung und pH-Verteilung in malignen Tumoren—Biologische und therapeutische Aspekte. *In: B. Bromm, and D. W. Luebbers (eds.), Physiologie aktuell*, Vol. 1, pp. 53-67. Stuttgart: Gustav Fischer Verlag, 1986.
67. Vaupel, P., and Kallinowski, F. Hemoconcentration of blood flowing through human tumor xenografts. *Int. J. Microcirc. Clin. Exp.*, **6**: 72, 1987.
68. Butler, T. P., Grantham, F. H., and Gullino, P. M. Bulk transfer of fluid in the interstitial compartment of mammary tumors. *Cancer Res.*, **35**: 512-516, 1975.
69. Seveck, E. M., and Jain, R. K. Blood flow and venous pH of tissue-isolated Walker 256 carcinoma during hyperglycemia. *Cancer Res.*, **48**: 1201-1207, 1988.
70. Warburg, O. *The Metabolism of Tumors*. London: Arnold Constable, 1930.
71. Wendling, P., Vaupel, P., Fischer, J., and Brünner, H. Splenic respiratory gas exchange and glucose uptake in patients with splenomegaly in hypersplenism and Hodgkin's disease. *Klin. Wochenschr.*, **55**: 1057-1061, 1977.
72. Aisenberg, A. C. *The Glycolysis and Respiration of Tumors*. New York: Academic Press, 1961.
73. Alvarez, E., Okagaki, T., and Richart, F. M. Oxygen consumption of endometrial adenocarcinoma. *Am. J. Obstet. Gynecol.*, **109**: 874-878, 1971.
74. Constable, T. B., Rogers, M. A., and Evans, N. T. S. Comparison between the oxygen removal rate and the histological structure of normal and tumour tissues. *Pfluegers Arch. Gesamte Physiol. Menschen Tiere*, **373**: 145-157, 1978.
75. Macbeth, R. A. L., and Bekesi, J. G. Oxygen consumption and anaerobic glycolysis of human malignant and normal tissue. *Cancer Res.*, **22**: 244-248, 1962.
76. Shapot, V. S. *Biochemical Aspects of Tumour Growth*. Moscow: MIR Publishers, 1980.
77. Grote, J., Süsskind, R., and Vaupel, P. Oxygen diffusivity in tumor tissue (DS-carcinoma) under temperature conditions within the range of 20-40°C. *Pfluegers Arch. Gesamte Physiol. Menschen Tiere*, **372**: 37-42, 1977.
78. Vaupel, P. Effect of percentage water content in tissues and liquids on the diffusion coefficients of O<sub>2</sub>, CO<sub>2</sub>, N<sub>2</sub>, and H<sub>2</sub>. *Pfluegers Arch. Gesamte Physiol. Menschen Tiere*, **361**: 201-204, 1976.
79. Vaupel, P. Hypoxia in neoplastic tissue. *Microvasc. Res.*, **13**: 399-408, 1977.
80. Vaupel, P. Oxygen supply to malignant tumors. *In: H.-I. Peterson (ed.),*

- Tumor Blood Circulation: Angiogenesis, Vascular Morphology and Blood Flow of Experimental and Human Tumors, pp. 143-168. Boca Raton, FL: CRC Press, 1979.
81. Vaupel, P., Okunieff, P., Kallinowski, F., and Neuringer, L. J. Correlations between  $^{31}\text{P}$ -NMR spectroscopy and tissue  $\text{O}_2$  tension measurements in a murine fibrosarcoma. *Radiat. Res.*, in press, 1989.
  82. Vaupel, P., Okunieff, P., and Neuringer, L. J. Blood flow, tissue oxygenation, pH distribution, and energy metabolism of murine mammary adenocarcinomas during growth. *Adv. Exp. Med. Biol.*, 248: 835-845, 1989.
  83. Vaupel, P., Wendling, P., Thomé, H., and Fischer, J. Atemgaswechsel und Glucoseaufnahme der menschlichen Milz *in situ*. *Klin. Wochenschr.*, 55: 239-242, 1977.
  84. Cater, D. B., and Silver, I. A. Quantitative measurements of oxygen tensions in normal tissues and in the tumours of patients before and after radiotherapy. *Acta Radiol.*, 53: 233-256, 1960.
  85. Ernst, E. A., Nelson, D., and DePalma, R. Tissue blood flow and oxygenation during large vessel surgery. *Adv. Exp. Med. Biol.*, 75: 663-666, 1976.
  86. Gatenby, R. A., Coia, L. R., Richter, M. P., Katz, H., Moldofsky, P. J., Engstrom, P., Brown, D. Q., Brookland, R., and Broder, G. J. Oxygen tension in human tumours: *in vivo* mapping using CT-guided probes. *Radiology*, 156: 211-214, 1985.
  87. Gatenby, R. A., Kessler, H. B., Rosenblum, J. S., Coia, L. R., Moldofsky, P. J., Hartz, W. H., and Broder, G. J. Oxygen distribution in squamous cell carcinoma metastases and its relationship to outcome of radiation therapy. *Int. J. Radiat. Oncol. Biol. Phys.*, 14: 831-838, 1988.
  88. Jamieson, D., and van den Brenk, H. A. S. Oxygen tension in human malignant disease under hyperbaric conditions. *Br. J. Cancer*, 19: 139-150, 1965.
  89. Weiss, C., and Fleckenstein, W. Local tissue  $\text{pO}_2$  measured with "thick" needle probes. *Funktionsanal. Biol. Syst.*, 15: 155-166, 1986.
  90. Endrich, B. Hyperthermie und Tumormikrozirkulation. *Beitr. Onkol.*, 31: 1-138, 1988.
  91. Kolstad, P. Intercapillary distance, oxygen tension and local recurrence in cervix cancer. *Scand. J. Clin. Lab. Invest. Suppl.*, 106: 145-157, 1968.
  92. Ehrly, A. M., and Schroeder, W. Zur Pathophysiologie der chronischen arteriellen Verschlusskrankheit. *Herz/Kreisl.*, 11: 275-281, 1979.
  93. Fleckenstein, W., Reinhart, K., Kersting, T., Denhardt, R., Jasper, A., Weiss, C., and Eyrich, K. Dopamine effects on the oxygenation of human skeletal muscle. *Adv. Exp. Med. Biol.*, 180: 609-622, 1984.
  94. Kunze, K. Das Sauerstoffdruckfeld im normalen und pathologisch veränderten Muskel. Berlin: Springer-Verlag, 1969.
  95. Lund, N. Skeletal and cardiac muscle oxygenation. *Adv. Exp. Med. Biol.*, 191: 37-41, 1985.
  96. Wiener, L., Santamore, W. P., Venkataswamy, A., Plzak, L., and Templeton, J. Postoperative monitoring of myocardial oxygen tension: experience in 51 coronary artery bypass patients. *Clin. Cardiol.*, 5: 431-440, 1982.
  97. Fleckenstein, W., and Weiss, C. Ein neues Gewebe- $\text{pO}_2$ -Messverfahren zum Nachweis von Mikrozirkulationsstörungen. *Focus Med. Hochschule Lübeck*, 1: 74-84, 1984.
  98. Cooper, R., Crow, H. J., Walter, W. G., and Winter, A. L. Regional control of cerebral vascular reactivity and oxygen supply in man. *Brain Res.*, 3: 174-191, 1966.
  99. Roberts, M., and Owens, G. Direct mass spectrographic measurement of regional intracerebral oxygen, carbon dioxide, and argon. *J. Neurosurg.*, 37: 706-710, 1972.
  100. Silver, I. A. The significance of clinical assessment of brain tissue oxygenation in different pathological conditions: an overview. *Fed. Proc.*, 38: 2495-2500, 1979.
  101. Bergsjø, P., and Evans, J. C. Oxygen tension of cervical carcinoma during the early phase of external irradiation. *Scand. J. Clin. Lab. Invest.*, 27: 71-82, 1971.
  102. Evans, N. T. S., and Naylor, P. F. D. The effect of oxygen breathing and radiotherapy upon the tissue oxygen tension of some human tumours. *Br. J. Radiol.*, 36: 418-425, 1963.
  103. Cater, D. B. Oxygen tension in neoplastic tissues. *Tumori*, 50: 435-444, 1964.
  104. Pappova, N., Siracka, E., Vacek, A., and Durkovsky, J. Oxygen tension and prediction of the radiation response. Polarographic study in human breast cancer. *Neoplasma (Bratisl.)*, 29: 669-674, 1982.
  105. Badib, A. O., and Webster, J. H. Changes in tumor oxygen tension during radiation therapy. *Acta Radiol. Ther. Phys. Biol.*, 8: 247-257, 1969.
  106. Urbach, F., and Noell, W. K. Effects of oxygen breathing on tumor oxygen measured polarographically. *J. Appl. Physiol.*, 13: 61-65, 1958.
  107. Urbach, F. Pathophysiology of malignancy. I. Tissue oxygen tension of benign and malignant tumors of the skin. *Proc. Soc. Exp. Biol. Med.*, 92: 644-649, 1956.
  108. Awwad, H. K., El Nagar, M., Mocktar, N., and Barsoum, M. Intercapillary distance measurements as an indicator of hypoxia in carcinoma of the cervix uteri. *Int. J. Radiat. Oncol. Biol. Phys.*, 12: 1329-1333, 1986.
  109. Siracka, E., Revesz, L., Kovac, R., and Siracky, J. Vascular density in carcinoma of the uterine cervix and its predictive value for radiotherapy. *Int. J. Cancer*, 41: 819-822, 1988.
  110. Vaupel, P., Manz, R., Mueller-Klieser, W., and Grunewald, W. A. Intracapillary  $\text{HbO}_2$  saturation in malignant tumors during normoxia and hyperoxia. *Microvasc. Res.*, 17: 181-191, 1979.
  111. Mueller-Klieser, W., Vaupel, P., Manz, R., and Grunewald, W. A. Intracapillary oxyhemoglobin saturation in malignant tumours with central and peripheral blood supply. *Eur. J. Cancer*, 16: 195-201, 1980.
  112. Otte, J., Manz, R., Thews, G., and Vaupel, P. Impact of localized microwave hyperthermia on the oxygenation status of malignant tumors. *Adv. Exp. Med. Biol.*, 157: 49-55, 1982.
  113. Vaupel, P., Otte, J., and Manz, R. Oxygenation of malignant tumors after localized microwave hyperthermia. *Radiat. Environ. Biophys.*, 20: 289-300, 1982.
  114. Rofstad, E. K., DeMuth, P., Fenton, B. M., and Sutherland, R. M.  $^{31}\text{P}$  nuclear magnetic resonance spectroscopy studies of tumor energy metabolism and its relationship to intracapillary oxyhemoglobin saturation status and tumor hypoxia. *Cancer Res.*, 48: 5440-5446, 1988.
  115. Rofstad, E. K., Fenton, B. M., and Sutherland, R. M. Intracapillary  $\text{HbO}_2$  saturations in murine tumours and human tumour xenografts measured by cryospectrophotometry: relationship to tumour volume, tumour pH and fraction of radiobiologically hypoxic cells. *Br. J. Cancer*, 57: 494-502, 1988.
  116. Fenton, B. M., Rofstad, E. K., Degner, F. L., and Sutherland, R. M. Cryospectrophotometric determination of tumor intravascular oxyhemoglobin saturations: dependence on vascular geometry and tumor growth. *J. Natl. Cancer Inst.*, 80: 1612-1619, 1988.
  117. Vaupel, P., and Mueller-Klieser, W. Cell line and growth site as relevant parameters governing tumor tissue oxygenation. *Adv. Exp. Med. Biol.*, 208: 633-643, 1986.
  118. Wendling, P., Manz, R., Thews, G., and Vaupel, P. Inhomogeneous oxygenation of rectal carcinomas in humans. A critical parameter for preoperative irradiation? *Adv. Exp. Med. Biol.*, 180: 293-300, 1984.
  119. Vaupel, P., and Kallinowski, F. Tissue oxygenation of primary and xenotransplanted human tumours. In: E. M. Fielden, J. F. Fowler, J. H. Hendry, and D. Scott (eds.), *Radiation Research*, Vol. 2, pp. 707-712. London: Taylor & Francis, 1987.
  120. Mueller-Klieser, W., Vaupel, P., Manz, R., and Schmidseider, R. Intracapillary oxyhemoglobin saturation of malignant tumors in humans. *Int. J. Radiat. Oncol. Biol. Phys.*, 7: 1397-1404, 1981.
  121. Mlynek, M. L., van Beuningen, D., Leder, L. D., and Streffer, C. Measurement of the grade of vascularisation in histological tumour tissue sections. *Br. J. Cancer*, 52: 945-948, 1985.
  122. Gullino, P. M., and Grantham, F. H. Studies on the exchange of fluids between host and tumor. I. A method for growing "tissue-isolated" tumors in laboratory animals. *J. Natl. Cancer Inst.*, 27: 679-693, 1961.
  123. Vaupel, P. Atemgaswechsel und Glukosestoffwechsel von Implantationstumoren (DS-Carcinosarkom) *in vivo*. *Funktionsanal. Biol. Syst.*, 1: 1-138, 1974.
  124. Gullino, P. M., Grantham, F. H., and Courtney, A. H. Glucose consumption by transplanted tumors *in vivo*. *Cancer Res.*, 27: 1031-1040, 1967.
  125. Gullino, P. M., Grantham, F. H., Courtney, A. H., and Losonczy, I. Relationship between oxygen and glucose consumption by transplanted tumors *in vivo*. *Cancer Res.*, 27: 1041-1052, 1967.
  126. Grantham, F. H., Hill, D. M., and Gullino, P. M. Primary mammary tumors connected to the host by a single artery and vein. *J. Natl. Cancer Inst.*, 50: 1381-1383, 1973.
  127. Sauer, L. A., Stayman, J. W., and Dauchy, R. T. Amino acid, glucose, and lactic acid utilization *in vivo* by rat tumors. *Cancer Res.*, 42: 4090-4097, 1982.
  128. Sauer, L. A., and Dauchy, R. T. Ketone body, glucose, lactic acid, and amino acid utilization by tumors *in vivo* in fasted rats. *Cancer Res.*, 43: 3497-3503, 1983.
  129. Sauer, L. A., and Dauchy, R. T. Regulation of lactate production and utilization in rat tumors *in vivo*. *J. Biol. Chem.*, 260: 7496-7501, 1985.
  130. Sauer, L. A., and Dauchy, R. T. *In vivo* lactate production and utilization by Jensen sarcoma and Morris hepatoma. *Cancer Res.*, 46: 689-693, 1986.
  131. Kallinowski, F., Dave, S., Vaupel, P., Baessler, K. H., and Wagner, K. Glucose, lactate, and ketone body utilization by human mammary carcinomas *in vivo*. *Adv. Exp. Med. Biol.*, 191: 965-970, 1985.
  132. Kallinowski, F., Vaupel, P., Runkel, S., Berg, G., Fortmeyer, H. P., Baessler, K. H., Wagner, K., Mueller-Klieser, W., and Walenta, S. Glucose uptake, lactate release, ketone body turnover, metabolic micromilieu, and pH distribution in human breast cancer xenografts in nude mice. *Cancer Res.*, 48: 7264-7272, 1988.
  133. Richtsmeier, W. J., Dauchy, R., and Sauer, L. A. *In vivo* nutrient uptake by head and neck cancers. *Cancer Res.*, 47: 5230-5233, 1987.
  134. Di Chiro, G., Hatazawa, J., Katz, D. A., Rizzoli, H. V., and de Michele, D. J. Glucose utilization by intracranial meningiomas as an index of tumor aggressivity and probability of recurrence: a PET study. *Radiology*, 164: 521-526, 1987.
  135. Di Chiro, G., DeLaPaz, R. L., Brooks, R. A., Sokoloff, L., Kornblith, P. L., Smith, B. H., Patronas, N. J., Kufta, C. V., Kessler, R. M., Johnston, G. S., Manning, R. G., and Wolf, A. P. Glucose utilization of cerebral gliomas measured by [ $^{18}\text{F}$ ]fluoro deoxyglucose and positron emission tomography. *Neurology*, 32: 1323-1329, 1982.
  136. Di Chiro, G., Brooks, R. A., Patronas, N. J., Bairamian, D., Kornblith, P. L., Smith, B. H., Mansi, L., and Barker, J. Issues in the *in vivo* measurement of glucose metabolism of human central nervous system tumors. *Ann. Neurol.*, 15 (Suppl.): S138-S146, 1984.
  137. Patronas, N. J., Di Chiro, G., Brooks, R. A., DeLaPaz, R. L., Kornblith, P. L., Smith, B. H., Rizzoli, H. V., Kessler, R. M., Manning, R. G., Channing, M., Wolf, A. P., and O'Connor, C. M. [ $^{18}\text{F}$ ]fluoro deoxyglucose and positron emission tomography in the evaluation of radiation necrosis of the brain. *Radiology*, 144: 885-889, 1982.
  138. Kern, K. A., Brunetti, A., Norton, J. A., Chang, A. E., Malawer, M., Lack, E., Finn, R. D., Rosenberg, S. A., and Larson, S. M. Metabolic imaging of

- human extremity musculoskeletal tumors by PET. *J. Nucl. Med.*, 29: 181-186, 1988.
139. Nolop, K. B., Rhodes, C. G., Brudin, L. H., Beaney, R. P., Krausz, T., Jones, T., and Hughes, J. M. B. Glucose utilization *in vivo* by human pulmonary neoplasms. *Cancer (Phila.)*, 60: 2682-2689, 1987.
  140. Kuhl, D. E., Phelps, M. E., Kowell, A. P., Metter, E. J., Selin, C., and Winter, J. Effects of stroke on local cerebral metabolism and perfusion: mapping by emission computed tomography of  $^{18}\text{F}$ FDG and  $^{15}\text{NH}_3$ . *Ann. Neurol.*, 8: 47-60, 1980.
  141. Reivich, M., Kuhl, D., Wolf, A., Greenberg, J., Phelps, M., Ido, T., Casella, V., Fowler, J., Hoffman, E., Alavi, A., Som, P., and Sokoloff, L. The [ $^{18}\text{F}$ ]fluorodeoxyglucose method for the measurement of local cerebral glucose utilization in man. *Circ. Res.*, 44: 127-137, 1979.
  142. Phelps, M. E., Huang, S. C., Hoffman, E. J., Selin, C., Sokoloff, L., and Kuhl, D. E. Tomographic measurement of local cerebral glucose metabolic rate in humans with (F-18) 2-fluoro-2-deoxy-D-glucose: validation of method. *Ann. Neurol.*, 6: 371-388, 1979.
  143. Huang, S.-C., Phelps, M. E., Hoffman, E. J., Sideris, K., Selin, C. J., and Kuhl, D. E. Noninvasive determination of local cerebral metabolic rate of glucose in man. *Am. J. Physiol.*, 238: E69-E82, 1980.
  144. Mazziotta, J. C., Phelps, M. E., Miller, J., and Kuhl, D. E. Tomographic mapping of human cerebral metabolism: normal unstimulated state. *Neurology*, 31: 503-516, 1981.
  145. Baxter, L. R., Mazziotta, J. C., Phelps, M. E., Selin, C. E., Guze, B. H., and Fairbanks, L. Cerebral glucose metabolic rates in normal human females versus normal males. *Psychiatr. Res.*, 21: 237-245, 1987.
  146. Barlett, E. J., Brodie, J. D., Wolf, A. P., Christman, D. R., Laska, E., and Meissner, M. Reproducibility of cerebral glucose metabolic measurements in resting human subjects. *J. Cerebral Blood Flow Metab.*, 8: 502-512, 1988.
  147. Barlett, E. J., Brown, J. W., Wolf, A. P., and Brodie, J. P. Correlations between glucose metabolic rates in brain regions of healthy male adults at rest and during language stimulation. *Brain Language*, 32: 1-18, 1987.
  148. Gambhir, S. S., Schwaiger, M., Huang, S. C., Krivokapich, J., Schelbert, H. R., Nienaber, C. A., and Phelps, M. E. Simple noninvasive quantification method for measuring myocardial glucose utilization in humans employing positron emission tomography and fluorine-18 deoxyglucose. *J. Nucl. Med.*, 30: 359-366, 1989.
  149. Schober, O., Meyer, G.-J., Duden, C., Lauenstein, L., Niggemann, J., Mueller, J.-A., Gaab, M. R., Becker, H., Dietz, H., and Hundeshagen, H. Die Aufnahme von Aminosäuren in Hirntumoren mit der Positronen-Emissionstomographie als Indikator für die Beurteilung von Stoffwechsellaktivität und Malignität. *Fortschr. Roentgenstr.*, 147: 503-509, 1987.
  150. Kallinowski, F., Runkel, S., Fortmeyer, H. P., Foerster, H., and Vaupel, P. L-Glutamine: a major substrate for tumor cells *in vivo*? *J. Cancer Res. Clin. Oncol.*, 113: 208-215, 1987.
  151. Mueller-Klieser, W., Walenta, S., Paschen, W., Kallinowski, F., and Vaupel, P. Metabolic imaging in microregions of tumors and normal tissues with bioluminescence and photon counting. *J. Natl. Cancer Inst.*, 80: 842-848, 1988.
  152. Rauen, H. M., Friedrich, M., and Norpoth, K. Die Beziehung zwischen Milchsäurekonzentration und Gewebe- pH beim DS-Carcinosarkom der Ratte. *Z. Naturforsch.*, 23b: 1018-1020, 1968.
  153. Albers, C., van den Kerckhoff, W., Vaupel, P., and Mueller-Klieser, W. Effect of CO<sub>2</sub> and lactic acid on intracellular pH of ascites tumor cells. *Respir. Physiol.*, 45: 273-285, 1981.
  154. Kallinowski, F., Tyler, G., Mueller-Klieser, W., and Vaupel, P. Growth-related changes of oxygen consumption rates of tumor cells grown *in vitro* and *in vivo*. *J. Cell. Physiol.*, 138: 183-191, 1989.
  155. Pampus, F. Die Wasserstoffionenkonzentration des Hirngewebes bei raumfordernden intracraniellen Prozessen. *Acta Neurochir.*, 11: 305-318, 1963.
  156. Ashby, B. S. pH studies in human malignant tumours. *Lancet*, 2: 312-315, 1966.
  157. Thistlethwaite, A. J., Leeper, D. B., Moylan, D. J., and Nerlinger, R. E. pH distribution in human tumors. *Int. J. Radiat. Oncol. Biol. Phys.*, 11: 1647-1652, 1985.
  158. Wike-Hooley, J. L., van den Berg, A. P., van der Zee, J., and Reinhold, H. S. Human tumour pH and its variation. *Eur. J. Cancer Clin. Oncol.*, 21: 785-791, 1985.
  159. van den Berg, A. P., Wike-Hooley, J. L., van den Berg-Blok, A. E., van der Zee, J., and Reinhold, H. S. Tumour pH in human mammary carcinoma. *Eur. J. Cancer Clin. Oncol.*, 18: 457-462, 1982.
  160. Inch, W. R. Direct current potential and pH of several varieties of skin neoplasms. *Can. J. Biochem. Physiol.*, 32: 519-525, 1954.
  161. Meyer, K. A., Kammerling, E. M., Amtman, L., Koller, M., and Hoffman, S. J. pH studies of malignant tissues in human beings. *Cancer Res.*, 8: 513-518, 1948.
  162. Millet, H. Measurements of the pH of normal, fetal, and neoplastic tissues by means of the glass electrode. *J. Biol. Chem.*, 78: 281-288, 1923.
  163. Naeslund, J., and Swenson, K.-E. Investigations on the pH of malignant tumours in mice and humans after the administration of glucose. *Acta Obstet. Gynecol. Scand.*, 32: 359-367, 1953.
  164. Okuneff, N. Über das Säure-Basengleichgewicht bei den Prozessen des Tumorzustands. *Z. Krebsforsch.*, 38: 283-288, 1933.
  165. Couch, N. P., Dmochowski, J. R., van de Water, J. M., Harken, D. E., and Moore, F. D. Muscle surface pH as an index of peripheral perfusion in man. *Ann. Surg.*, 173: 173-183, 1971.
  166. Laks, H., Dmochowski, J. R., and Couch, N. P. The relationship between muscle surface pH and oxygen transport. *Ann. Surg.*, 183: 193-198, 1976.
  167. O'Donnell, T. F. Measurement of percutaneous muscle surface pH. *Lancet*, 2: 533, 1975.
  168. O'Donnell, T. F., Raines, J. K., and Darling, R. C. Relationship of muscle surface pH to noninvasive hemodynamic studies. *Arch. Surg.*, 114: 600-604, 1979.
  169. Pineyro, J. R. Muscle pH monitoring. *J. Pediatr. Surg.*, 14: 77-79, 1979.
  170. Rithalia, S. V. S., Hewer, A. J. H., Tinker, J., and Herbert, P. Continuous tissue pH measurement in critically ill adults with a miniaturized glass electrode. *J. Biomed. Eng.*, 2: 126-128, 1980.
  171. Harrison, D. K., and Walker, W. F. Micro-electrode measurement of skin pH in humans during ischemia, hypoxia and local hypothermia. *J. Physiol. (Lond.)*, 291: 339-350, 1979.
  172. Harrison, D. K., Spence, V. A., Beck, J. S., Lowe, J. G., and Walker, W. F. pH changes in the dermis during the course of the tuberculin skin test. *Immunology*, 59: 497-501, 1986.
  173. Stamm, O., Latscha, U., Janecek, P., and Campana, A. Development of a special electrode for continuous subcutaneous pH measurements in the infant scalp. *Am. J. Obstet. Gynecol.*, 124: 193-195, 1976.
  174. Meehan, S. E., and Walker, W. F. Measurements of tissue pH in skin by glass microelectrodes. *Lancet*, 2: 70-71, 1979.
  175. Warth, J. A., Desforges, J. F., and Stolberg, S. Intraerythrocyte pH, pCO<sub>2</sub> and the hexose monophosphate shunt. *Br. J. Haematol.*, 37: 373-377, 1977.
  176. Rottenberg, D. A., Ginos, J. Z., Kearfott, K. J., Junck, L., and Bigner, D. D. *In vivo* measurements of regional brain tissue pH using positron emission tomography. *Ann. Neurol.*, 15 (Suppl.): S98-S102, 1984.
  177. Hawkins, R. A., and Phelps, M. E. PET in clinical oncology. *Cancer Metastasis Rev.*, 7: 119-142, 1988.
  178. Syrota, A., Samson, Y., Boullais, C., Wajnberg, P., Loc'h, C., Crouzel, C., Maziere, B., Soussaline, F., and Baron, J. C. Tomographic mapping of brain intracellular pH and extracellular water space in stroke patients. *J. Cerebral Blood Flow Metab.*, 5: 358-368, 1985.
  179. Brooks, D. J., Lammertsma, A. A., Beaney, R. P., Leenders, K. L., Buckingham, P. D., Marshall, J., and Jones, T. Measurement of regional cerebral pH in human subjects using continuous inhalation of  $^{14}\text{CO}_2$  and positron emission tomography. *J. Cerebral Blood Flow Metab.*, 4: 458-465, 1984.
  180. Rottenberg, D. A., Ginos, J. Z., Kearfott, K. J., Junck, L., Dhawan, V., and Jarden, J. O. *In vivo* measurement of brain tumor pH using [ $^{11}\text{C}$ ]DMO and positron emission tomography. *Ann. Neurol.*, 17: 70-79, 1985.
  181. Junck, L., Blasberg, R., and Rottenberg, D. A. Brain and tumor pH in experimental leptomeningeal carcinomatosis. *Trans. Am. Neurol. Assoc.*, 106: 298-301, 1981.
  182. Daly, P. F., and Cohen, J. S. Magnetic resonance spectroscopy of tumors and potential *in vivo* clinical applications: a review. *Cancer Res.*, 49: 770-779, 1989.
  183. Bottomley, P. A. Human *in vivo* NMR spectroscopy in diagnostic medicine: clinical tool or research probe? *Radiology*, 170: 1-15, 1989.
  184. Ng, T. C., Vijayakumar, S., Majors, A. W., Thomas, F. J., Meaney, T. F., and Baldwin, N. J. Response of a non-Hodgkin lymphoma to  $^{60}\text{Co}$  therapy monitored by  $^{31}\text{P}$  MRS *in situ*. *Int. J. Radiat. Oncol. Biol. Phys.*, 13: 1545-1551, 1987.
  185. Griffiths, J. R., Cady, E., Edwards, R. H. T., McCready, V. R., Wilkie, D. R., and Wiltshaw, E.  $^{31}\text{P}$ -NMR studies of a human tumour *in situ*. *Lancet*, 1: 1435-1436, 1983.
  186. Evelhoch, J. L., Sapareto, S. A., Jick, D. E. L., and Ackerman, J. J. H. *In vivo* metabolic effects of hyperglycemia in murine radiation-induced fibrosarcoma: a  $^{31}\text{P}$ -NMR investigation. *Proc. Natl. Acad. Sci. USA*, 81: 6496-6500, 1984.
  187. Moon, R. B., and Richards, J. H. Determination of intracellular pH by  $^{31}\text{P}$  magnetic resonance. *J. Biol. Chem.*, 248: 7276-7278, 1973.
  188. Nidecker, A. C., Mueller, S., Aue, W. P., Seelig, J., Fridrich, R., Remagen, W., Hartweg, H., and Benz, U. F. Extremity bone tumors: Evaluation by P-31 MR spectroscopy. *Radiology*, 157: 167-174, 1985.
  189. Semmler, W., Gademann, G., Bachert-Baumann, P., Bier, V., Zabel, H.-J., Lorenz, W. J., and van Kaick, G. *In vivo*  $^{31}\text{P}$  Phosphor-Spektroskopie von Tumoren: Prä-, intra- und posttherapeutisch. *Fortschr. Röntgenstr.*, 149: 369-377, 1988.
  190. Semmler, W., Gademann, G., Bachert-Baumann, P., Zabel, H.-J., Lorenz, W. J., and van Kaick, G. Monitoring human tumor response to therapy by means of P-31 MR spectroscopy. *Radiology*, 166: 533-539, 1988.
  191. Oberhaensli, R. D., Hilton-Jones, D., Bore, P. J., Hands, L. J., Rampling, R. P., and Radda, G. K. Biochemical investigation of human tumours *in vivo* with phosphorus-31 magnetic resonance spectroscopy. *Lancet*, 1: 8-11, 1986.
  192. Ng, T. C., Majors, A. W., Vijayakumar, S., Baldwin, N. J., Thomas, F. J., Koumoundouris, I., Taylor, M. E., Grundfest, S. F., Meaney, T. F., Tubbs, R. R., and Shin, K. H. Human neoplasm pH and response to radiation therapy: P-31 MR spectroscopy studies *in situ*. *Radiology*, 170: 875-878, 1989.
  193. Negendank, W., Crowley, M., Keller, N., Nussdorfer, M., and Evelhoch, J. L. *In vivo*  $^{31}\text{P}$  MRS of normal human breasts: age dependence and comparison with breast cancers. *In: Proceedings of the 7th Annual Meeting of the Society for Magnetic Resonance Medicine, San Francisco, Vol. 1, p. 336, 1988.*
  194. Sijens, P. E., Wijrdeman, H. K., Moerland, M. A., Bakker, C. J. G., Vermeulen, J. W. A. H., and Luyten, P. R. Human breast cancer *in vivo*: heat and P-31 MR spectroscopy at 1.5 T. *Radiology*, 169: 615-620, 1988.
  195. Arnold, D. L., Shoubridge, E. A., Feindel, W., and Villemure, J.-G. Meta-

- bolic changes in cerebral gliomas within hours of treatment with intra-arterial BCNU demonstrated by phosphorus magnetic resonance spectroscopy. *Can. J. Neurol. Sci.*, *14*: 570-575, 1987.
196. den Hollander, J. A., and Luyton, P. R. Image-guided localized <sup>1</sup>H and <sup>31</sup>P NMR spectroscopy of humans. *Ann. NY Acad. Sci.*, *508*: 386-398, 1987.
  197. Segebarth, C. M., Baleriaux, D. F., Arnold, D. L., Luyton, P. R., and den Hollander, J. A. MR image-guided P-31 MR spectroscopy in the evaluation of brain tumor treatment. *Radiology*, *165*: 215-219, 1987.
  198. Hubesch, B., Sappey-Mariniere, D., Roth, K., Sanuki, E., Hodes, J. E., Matson, G. B., and Weiner, M. W. Improved ISIS for studies of human brain and brain tumors. *In: Proceedings of the 7th Annual Meeting of the Society for Magnetic Resonance Medicine, San Francisco, Vol. 1, p. 348, 1988.*
  199. Cadoux-Hudson, T., Blackledge, M. J., Rajagopalan, B., Taylor, D. J., and Radda, G. K. Measurement of phosphorus metabolites in patients with intracranial tumours. *In: Proceedings of the 7th Annual Meeting of the Society for Magnetic Resonance Medicine, San Francisco, Vol. 2, p. 614, 1988.*
  200. Ng, T. C., Vijayakumar, S., Majors, A. W., Baldwin, N. J., Taylor, M. E., Thomas, F. J., Saxton, J. P., Meaney, T. F., Grundfest, S., and Tubbs, R. Examination of 31-P MRS metabolites and intracellular pH in 25 human neoplasms. *In: Proceedings of the 6th Annual Meeting of the Society for Magnetic Resonance Medicine, New York, Vol. 1, p. 104, 1987.*
  201. Ng, T. C., Majors, A. W., and Meaney, T. F. *In vivo* MR spectroscopy of human subjects with a 1.4-T whole body MR imager. *Radiology*, *158*: 517-520, 1986.
  202. Burt, C. T., Koutcher, J., Roberts, J. T., London, R. E., and Chance, B. Magnetic resonance spectroscopy of the musculoskeletal system. *Radiol. Clin. North Am.*, *24*: 321-331, 1986.
  203. Itoh, M., Kawahara, T., Yoshikawa, K., Jagi, K., Iio, M., Yamai, S., Iriguchi, N., and Maki, T. Measurement of *in vivo* dynamic metabolism of the athletes and overtraining runner by <sup>31</sup>P-NMR. *In: Proceedings of the 6th Annual Meeting of the Society for Magnetic Resonance Medicine, New York, Vol. 2, p. 552, 1987.*
  204. Gross, B., Kensora, T. G., Glasberg, M. R., Welch, K. M. A., and Smith, M. B. Early intracellular acidosis during exercise in sensory neuropathy: 31-P NMR spectroscopy study. *In: Proceedings of the 6th Annual Meeting of the Society for Magnetic Resonance Medicine, New York, Vol. 2, p. 1036, 1987.*
  205. Pan, J. W., Hamm, J. R., Rothman, D. L., and Shulman, R. G. Intracellular pH of human muscle by <sup>1</sup>H NMR. *In: Proceedings of the 7th Annual Meeting of the Society for Resonance Medicine, San Francisco, Vol. 1, p. 251, 1988.*
  206. Wilson, J. R., McCully, K. K., Mancini, D. M., Boden, B., and Chance, B. Relationship of muscular fatigue to pH and diprotonated P<sub>i</sub> in humans: A <sup>31</sup>P-NMR study. *J. Appl. Physiol.*, *64*: 2333-2339, 1988.
  207. Levine, S. R., Welch, K. M. A., Helpert, J. A., Bruce, R., Ewing, J. R., Kensora, T., and Smith, M. B. Cerebral cortical phosphate metabolism and pH in patients with multiple subcortical infarcts: a controlled study with 31-phosphorus NMR spectroscopy. *In: Proceedings of the 6th Annual Meeting of the Society for Magnetic Resonance Medicine, New York, Vol. 2, p. 1001, 1987.*
  208. Jensen, K. E., Thomsen, C., and Henriksen, O. *In vivo* measurement of intracellular pH in human brain during different tensions of carbon dioxide in arterial blood. A <sup>31</sup>P-NMR study. *Acta Physiol. Scand.*, *134*: 295-298, 1988.
  209. Segebarth, C., Grivegnee, A., Luyton, P. R., and den Hollander, J. A. <sup>31</sup>P MR spectroscopy of the human liver. Assessment of fructose metabolism. *In: Proceedings of the 6th Annual Meeting of the Society for Magnetic Resonance Medicine, New York, Vol. 2, p. 603, 1987.*
  210. Vermeulen, J. W. A. H., Luyton, P. R., van der Heijden, J. I., and den Hollander, J. A. Uncovering the P<sub>i</sub> signal in the *in vivo* <sup>31</sup>P NMR spectrum of the human heart. *In: Proceedings of the 7th Annual Meeting of the Society for Magnetic Resonance Medicine, San Francisco, Vol. 2, p. 833, 1988.*
  211. Resnick, L. M., Gupta, R. K., Sosa, R. E., and Corbett, M. L. Intracellular pH in human and experimental hypertension. *Proc. Natl. Acad. Sci. USA*, *84*: 7663-7667, 1987.
  212. Petersen, A., Jacobsen, J. P., and Høder, M. <sup>31</sup>P NMR measurements of intracellular pH in erythrocytes: direct comparison with measurements using freeze-thaw and investigation into the influence of ionic strength and Mg<sup>2+</sup>. *Magn. Reson. Med.*, *4*: 341-350, 1987.
  213. Iles, R. A., Stevens, A. N., and Griffiths, J. R. NMR studies of metabolites in living tissue. *Progr. Nucl. Magn. Reson. Spectrosc.*, *15*: 49-200, 1982.
  214. Roos, A., and Boron, W. F. Intracellular pH. *Physiol. Rev.*, *61*: 296-421, 1981.